Electronic Supplementary Information

Assembly-Controlled Supramolecular Aggregation-Induced Emission Systems based on Amphiphilic Block Polymer Hosts

Yu-Qi Zhu,[a] Zhong-Yuan Chen,[a] Zhi-Wei Zhou,[a] Zhaojun Chen,[a] Ming-Xue Wu,*[a] and Xing-Huo Wang*[a]*

[a]Institute for Sustainable Energy and Resources, College of Chemistry and Chemical Engineering, Qingdao University, 308 Ningxia Road, Qingdao 266071, P. R. China

E-mail: wxh93@qdu.edu.cn; wmx517@qdu.edu.cn; chenzhaojun@qdu.edu.cn

Content

1. Synthesis

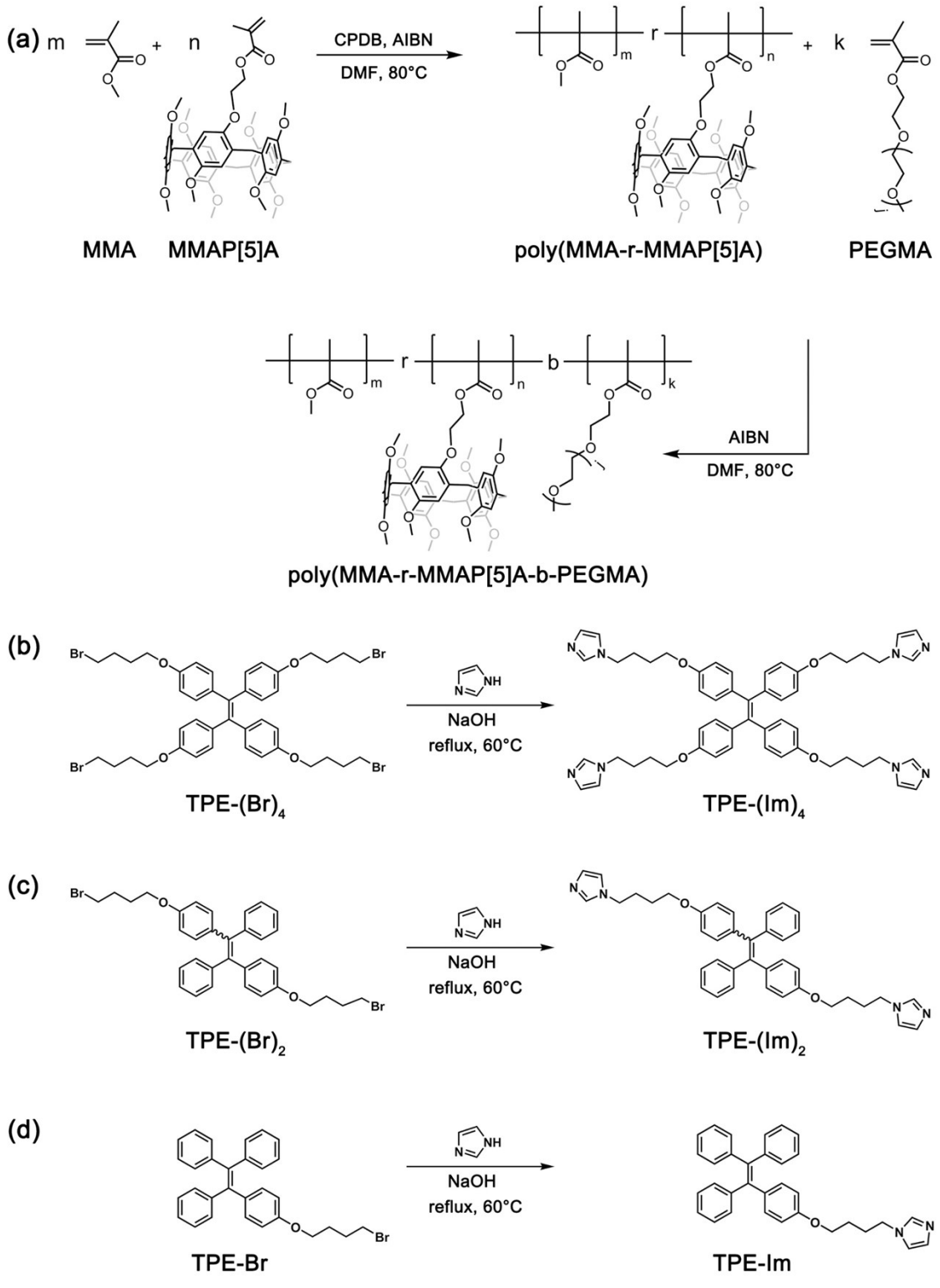

Fig. S1. Synthesatic routes to TPE derivatives with different number of guest moieties (TPE-$(Im)_4$, TPE-$(Im)_2$, TPE-Im) and amphiphilic block polymer hosts.

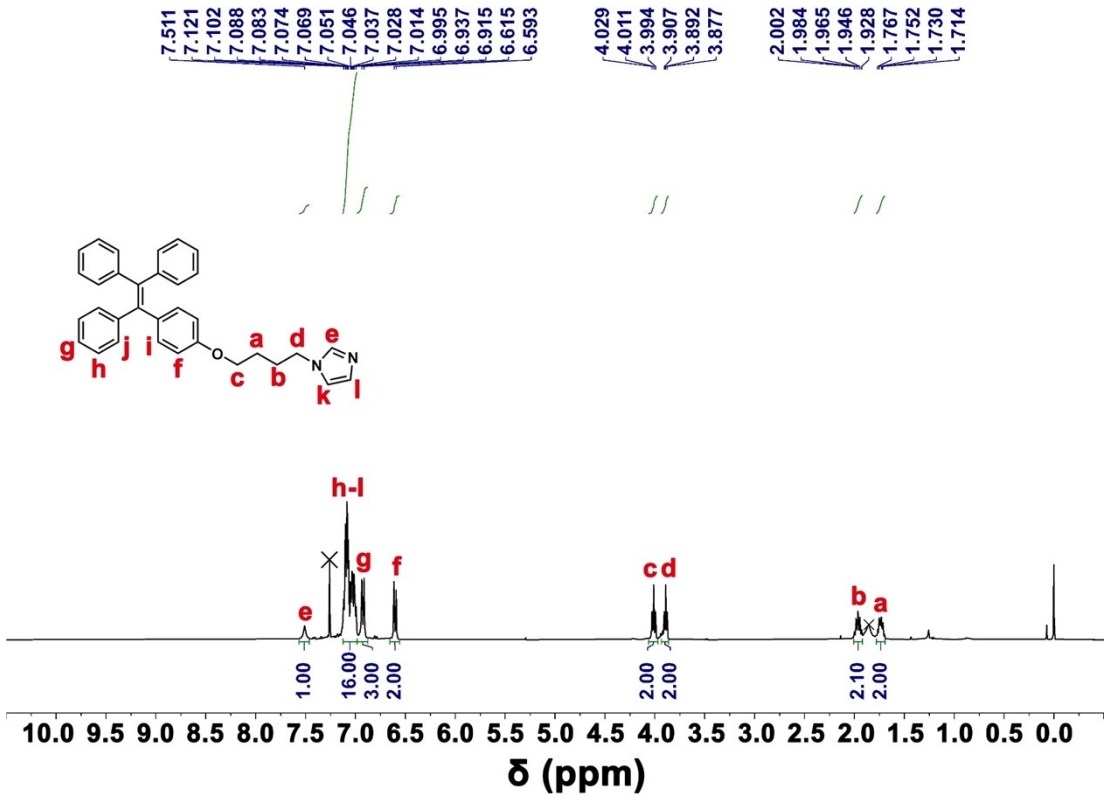

Fig. S2. ^{1}H NMR spectrum (400 MHz, $CDCl_3$, 298 K) of TPE-Im.

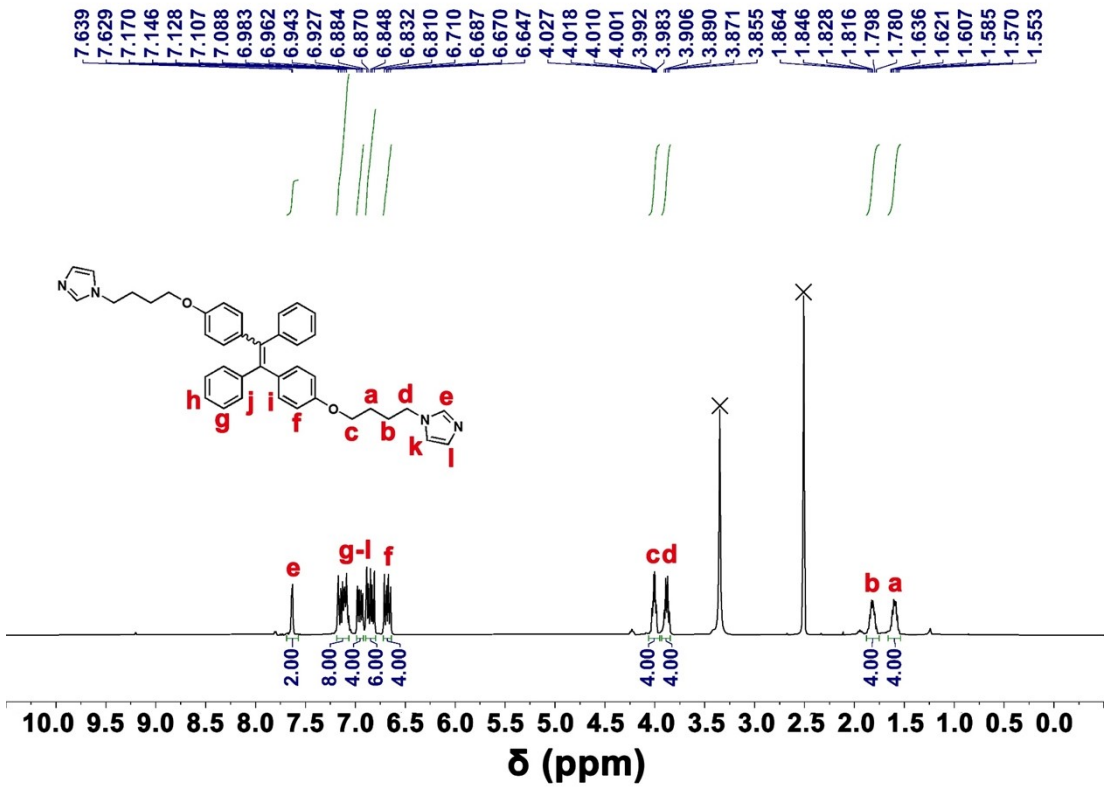

Fig. S3. ^{1}H NMR spectrum (400 MHz, DMSO-d_6, 298 K) of TPE-$(Im)_2$.

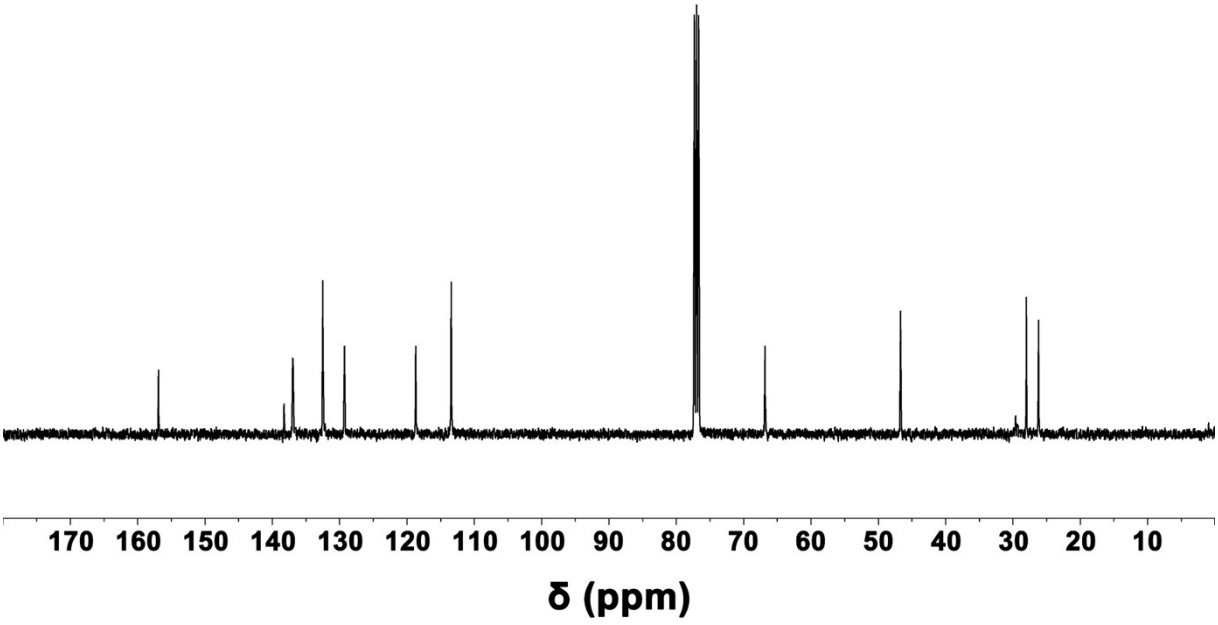

Fig. S4. ^{13}C NMR spectrum (101 MHz, $CDCl_3$, 298 K) of TPE-$(Im)_2$.

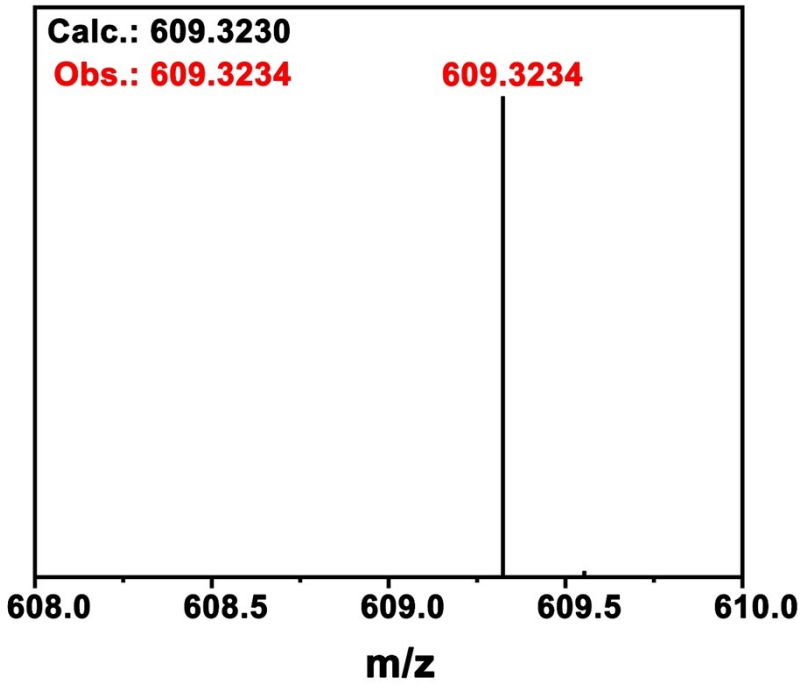

Fig. S5. HR-ESI-MS spectrum of TPE-$(Im)_2$.

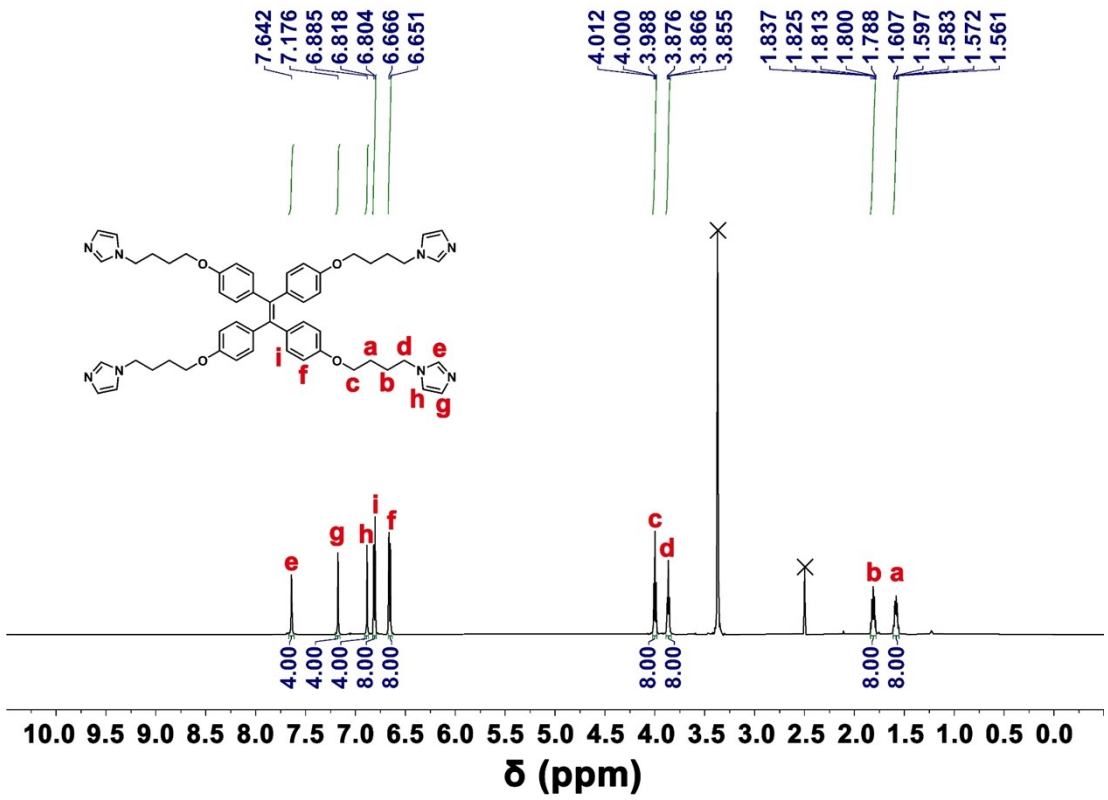

Fig. S6. ^{1}H NMR spectrum (600 MHz, DMSO-d_6, 298 K) of TPE-(Im)$_4$.

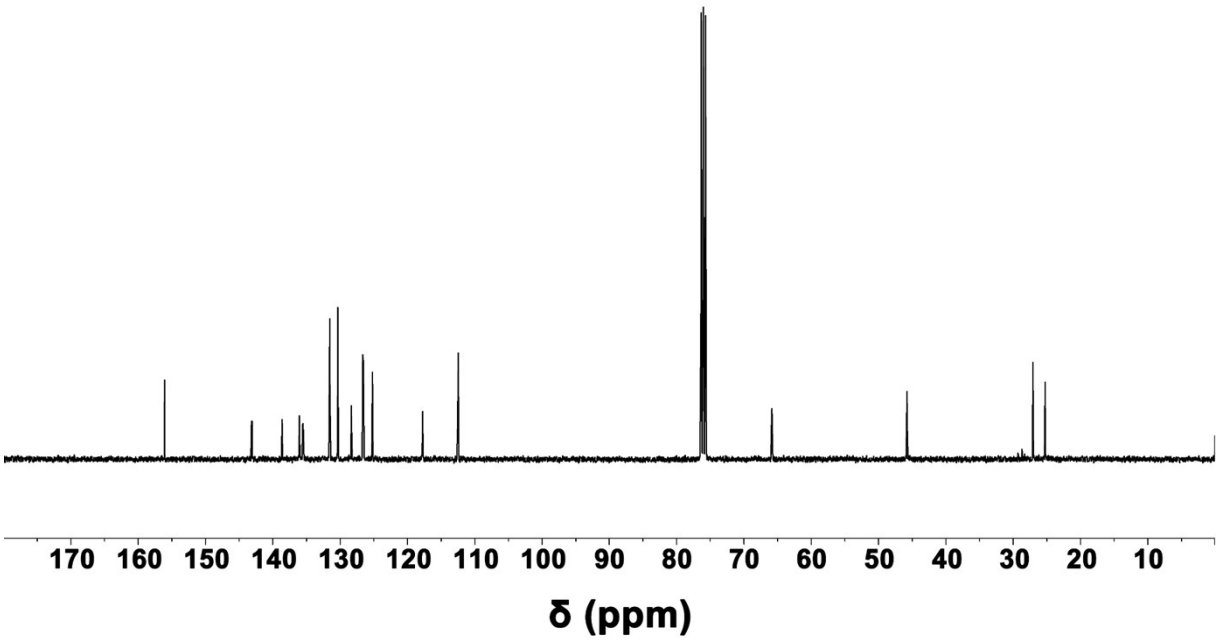

Fig. S7. ^{13}C NMR spectrum (101 MHz, $CDCl_3$, 298 K) of TPE-(Im)$_4$.

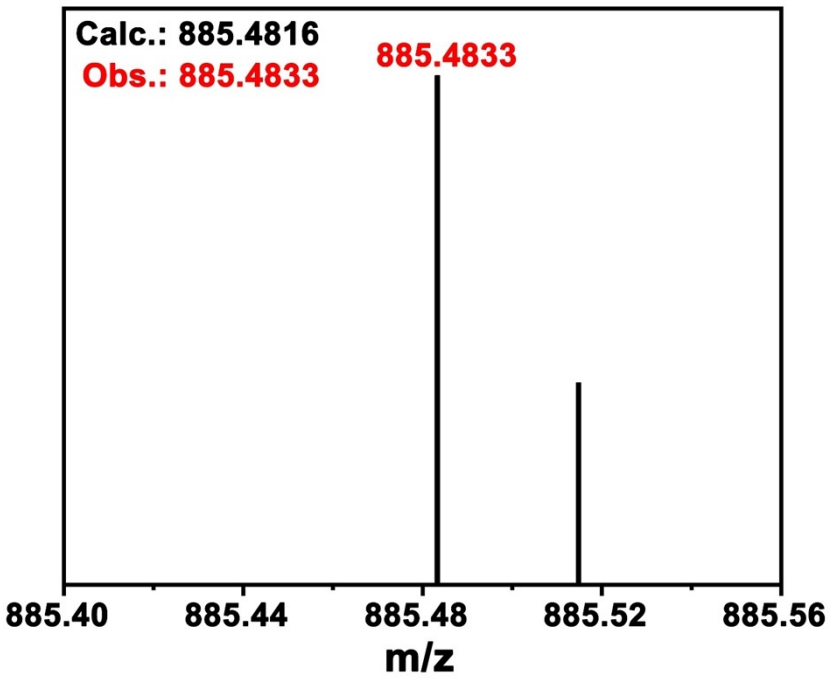

Fig. S8. HR-ESI-MS spectrum of TPE-$(Im)_4$.

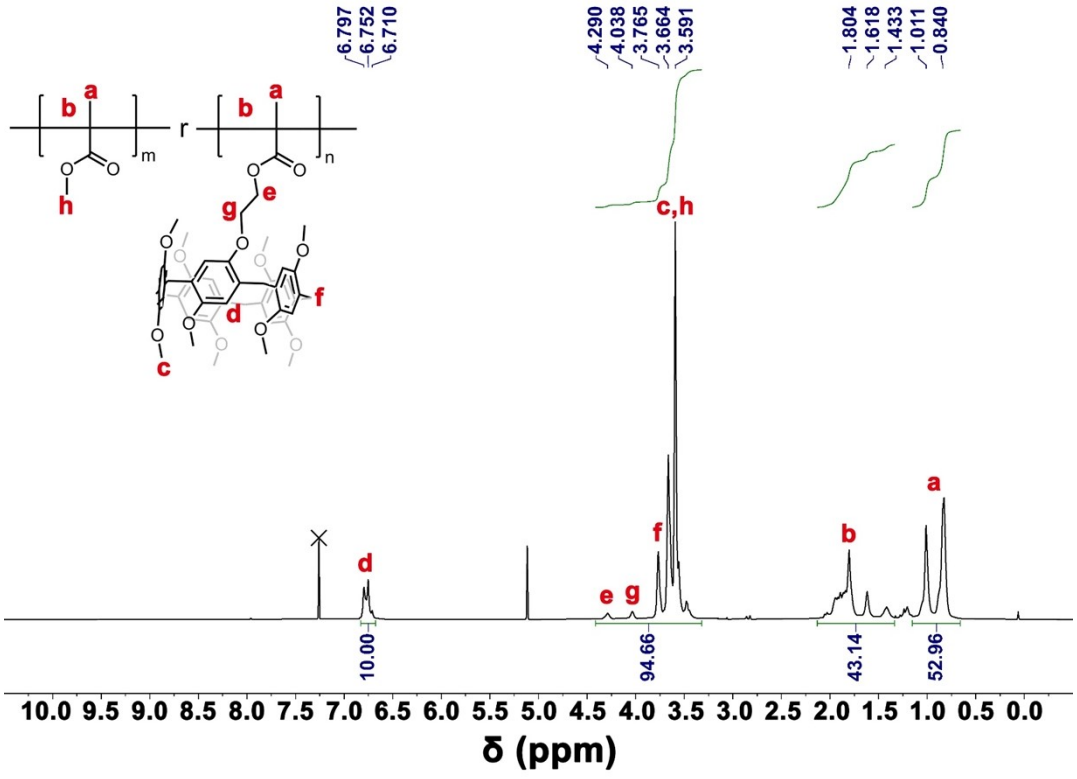

Fig. S9. ^{1}H NMR spectrum (600 MHz, $CDCl_3$, 298 K) of PH-a.

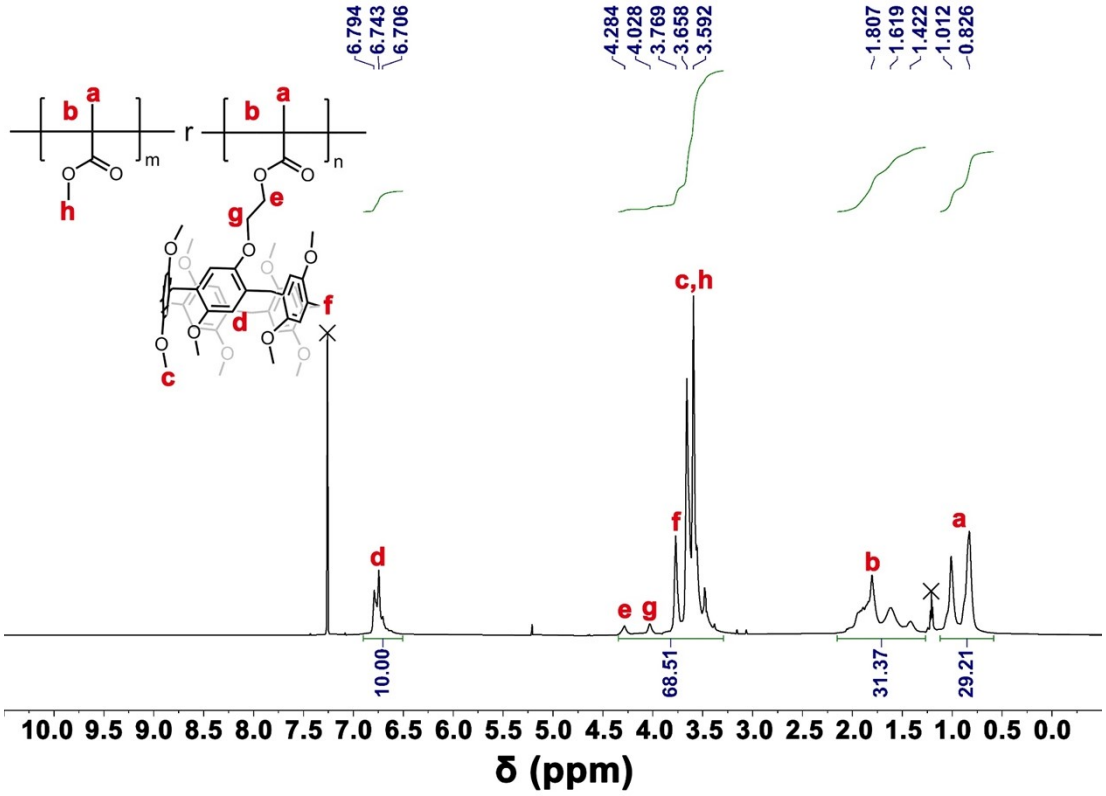

Fig. S10. ^{1}H NMR spectrum (600 MHz, $CDCl_3$, 298 K) of PH-b.

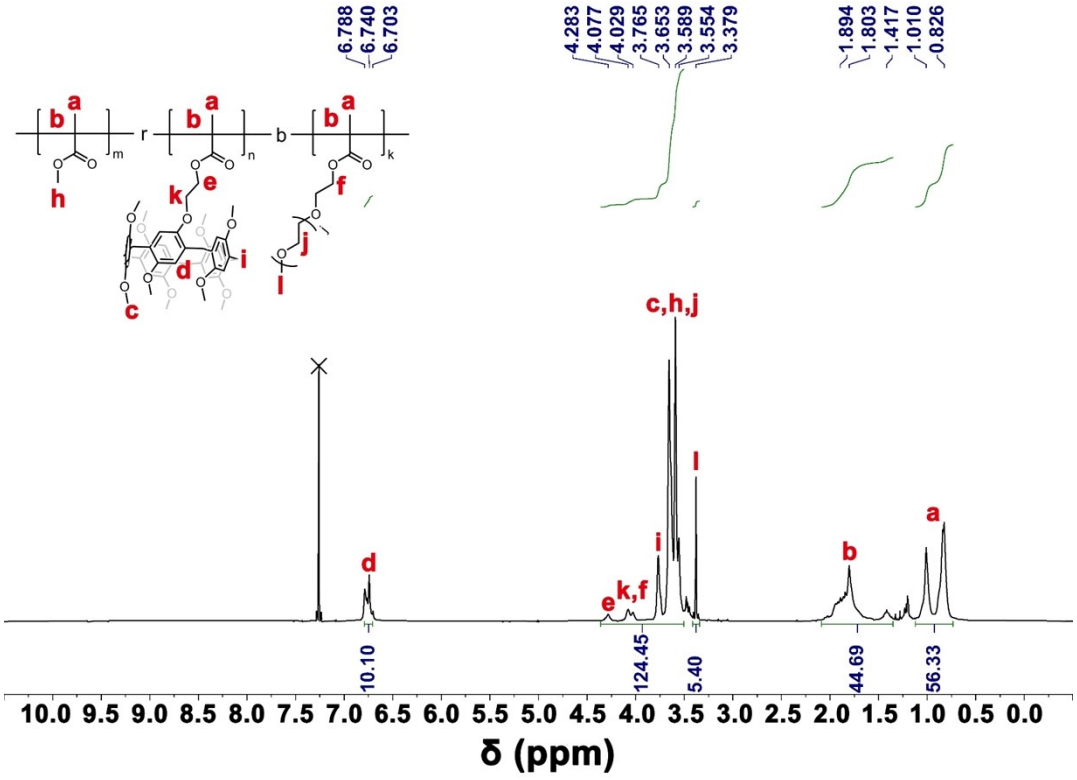

Fig. S11. ^{1}H NMR spectrum (600 MHz, $CDCl_3$, 298 K) of PH1.

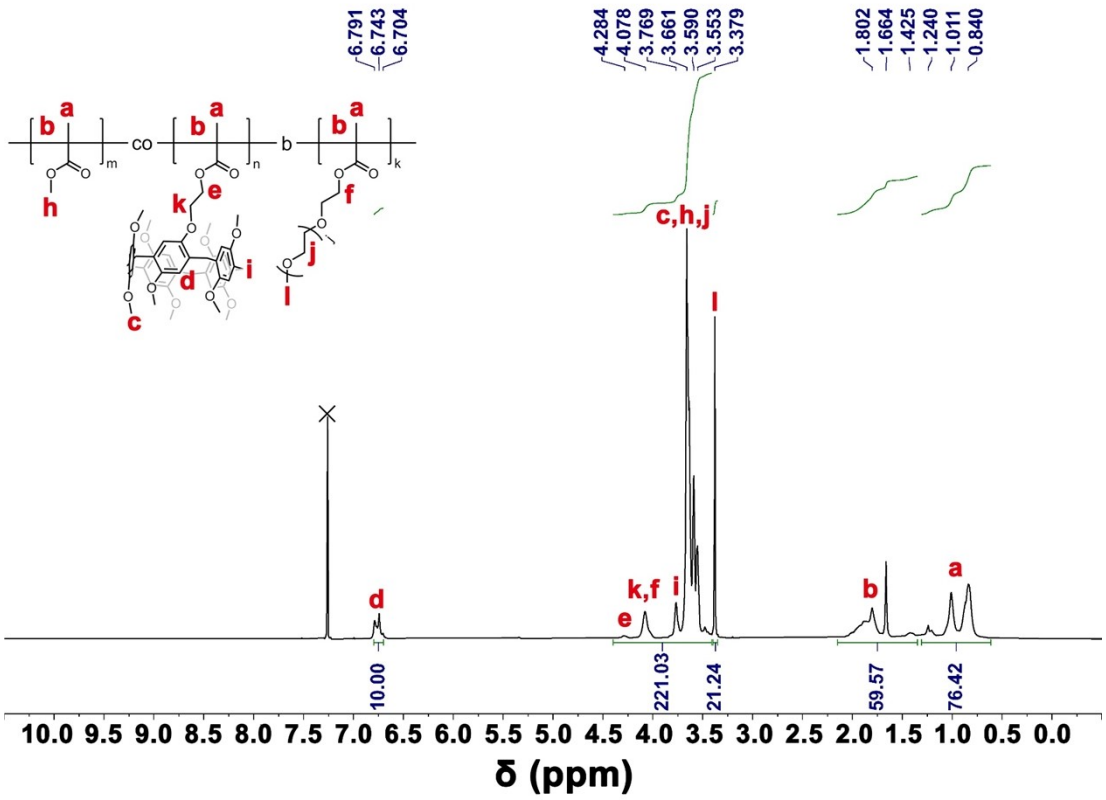

Fig. S12. ^{1}H NMR spectrum (600 MHz, $CDCl_3$, 298 K) of PH2.

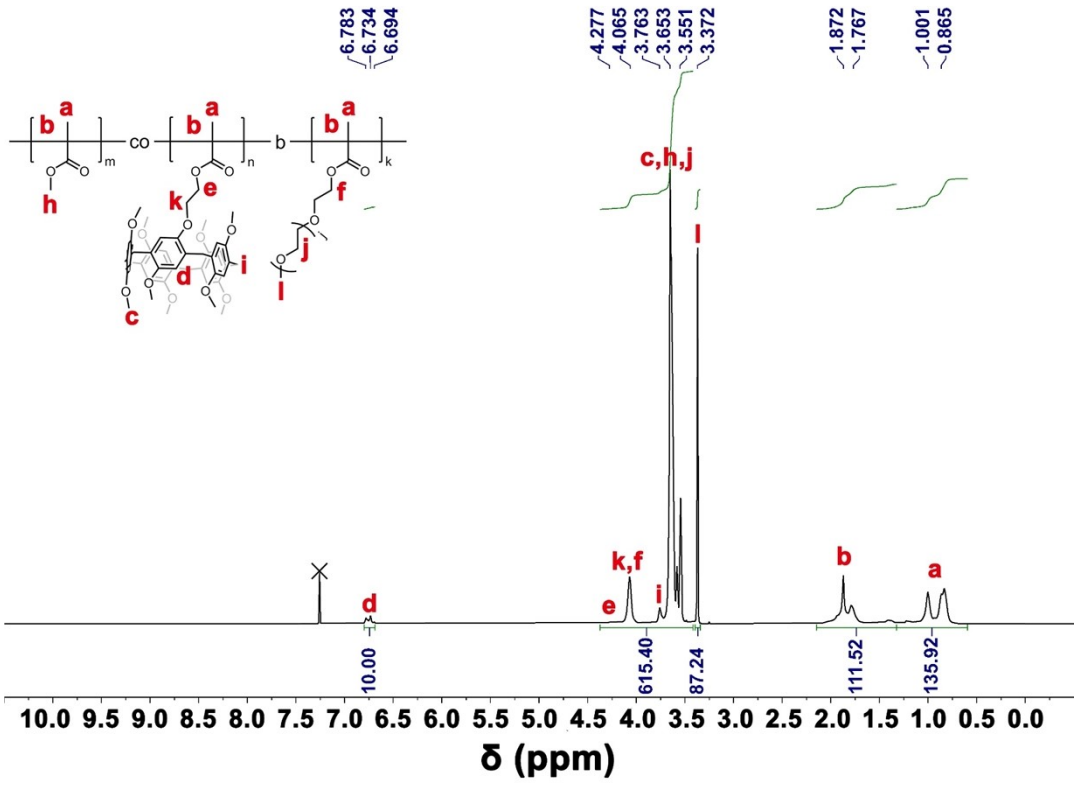

Fig. S13. ^{1}H NMR spectrum (600 MHz, $CDCl_3$, 298 K) of PH3.

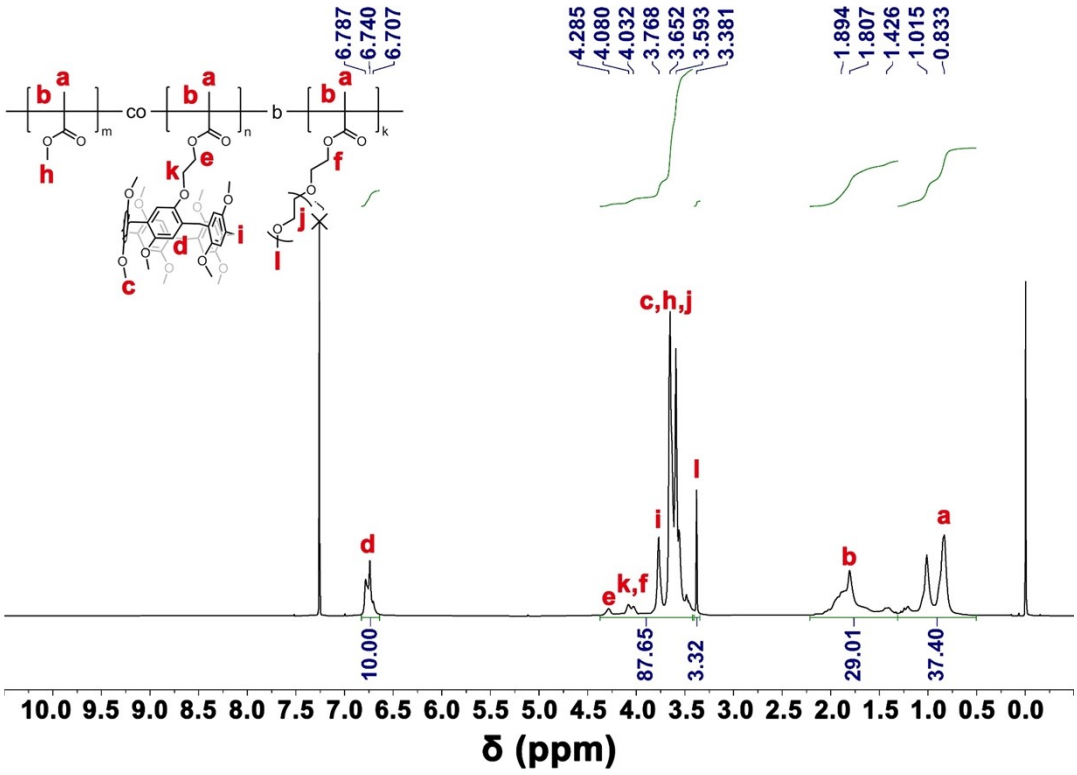

Fig. S14. ^{1}H NMR spectrum (600 MHz, $CDCl_3$, 298 K) of PH4.

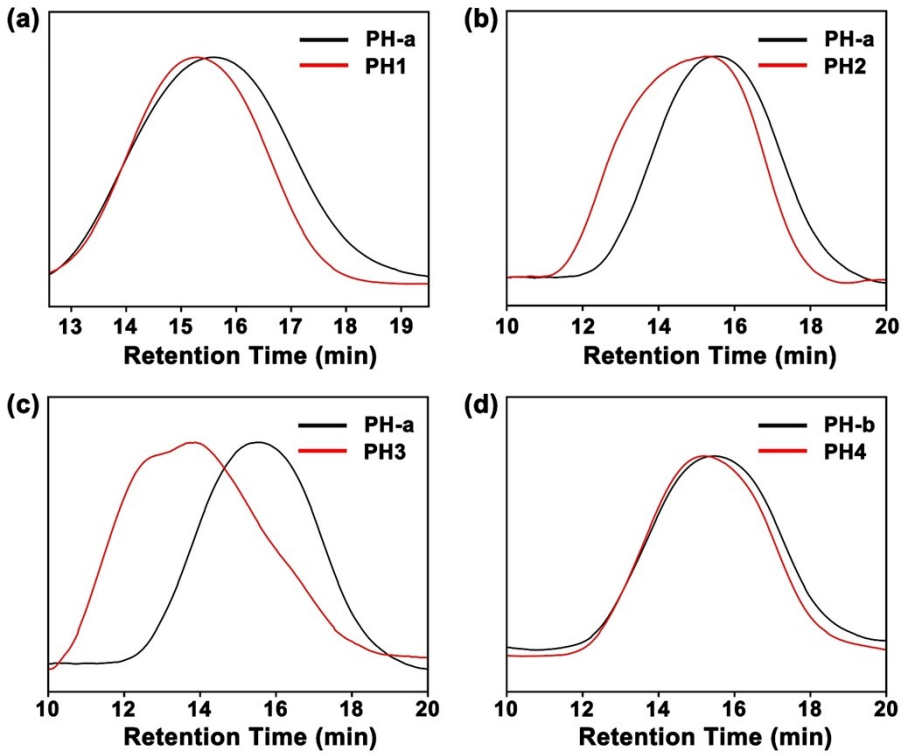

Fig. S15. (a) GPC traces of PH-a and PH1. (b) GPC traces of PH-a and PH2. (c) GPC traces of PH-a and PH3. (d) GPC traces of PH-b and PH4.

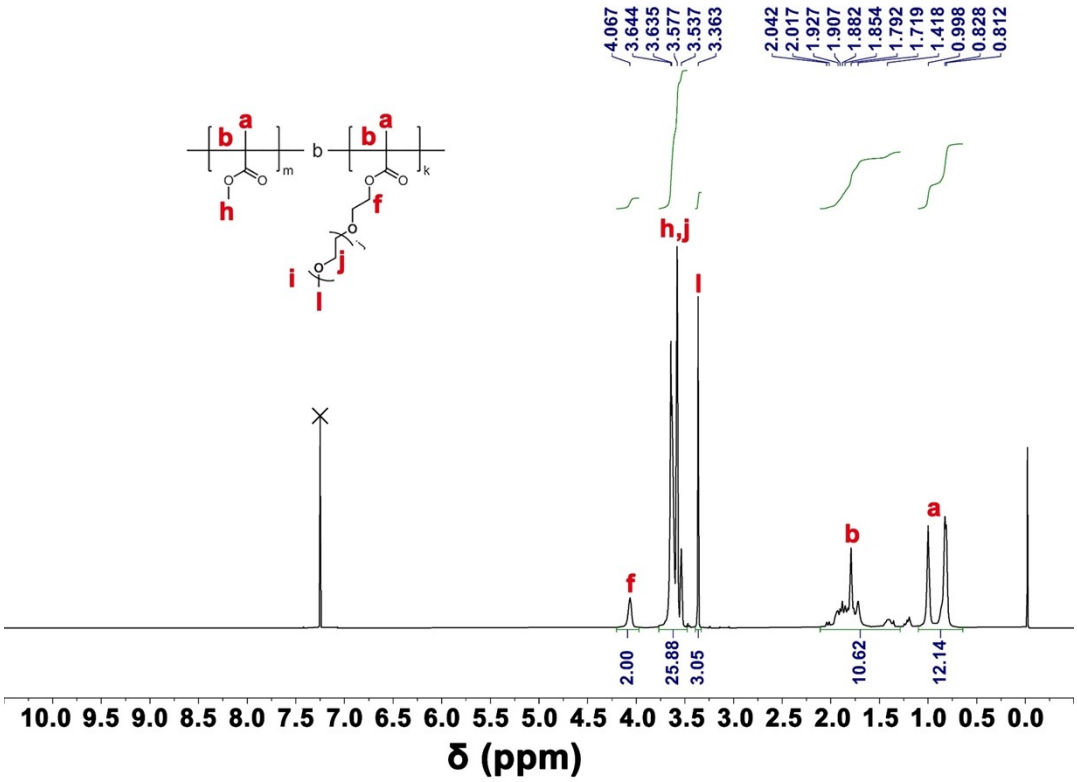

Fig. S16. ^{1}H NMR spectrum (600 MHz, $CDCl_3$, 298 K) of P-c.

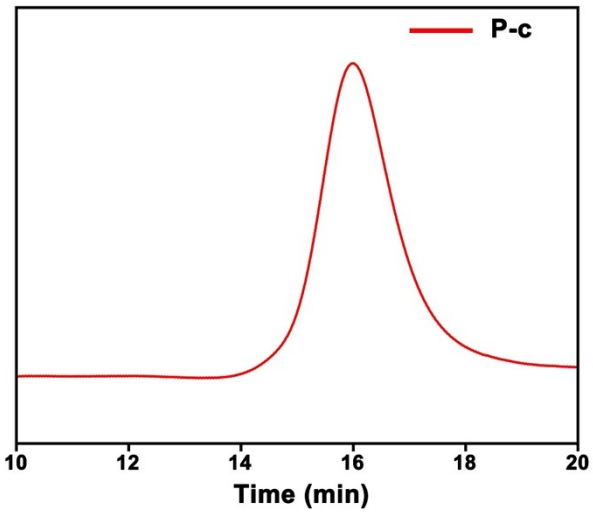

Fig. S17. GPC trace of P-c.

The ratio of repeating units in block polymer hosts was calculated by ^{1}H NMR spectra. Taking PH1 in Fig. S11 as an example, the integral area of benzene rings ascribed to pillar[5]arene units at 6.7-6.8 ppm was determined to be 10, in the meantime, the number of repeating units of $PEGMA_{300}$ was claculated by the signal appeared at 3.379 ppm corresponding to methoxy groups of $PEGMA_{300}$ ($5.4\ 3^{-1} = 1.8$). Finally, the number of repeating unit of MMA

was calculated to be 17 by the signals appeared at 3.55-4.3 ppm. As a result, the proportion among MMA, MMAP[5]A and $PEGMA_{300}$ of PH1 was calculated to be 200:11:21.

Similarly, the proportion among MMA, MMAP[5]A and $PEGMA_{300}$ of PH2, PH3 and PH4 was calculated to be 200:11:77, 200:11:319 and 200:22:24, respectively. The ratio of MMA to MMAP[5]A of PH-a and PH-b was calculated to be 200:11 and 200:22. The ratio of MMA to $PEGMA_{300}$ in P-c was calculated to be 200:67.

2. Characterization of host-guest interactions

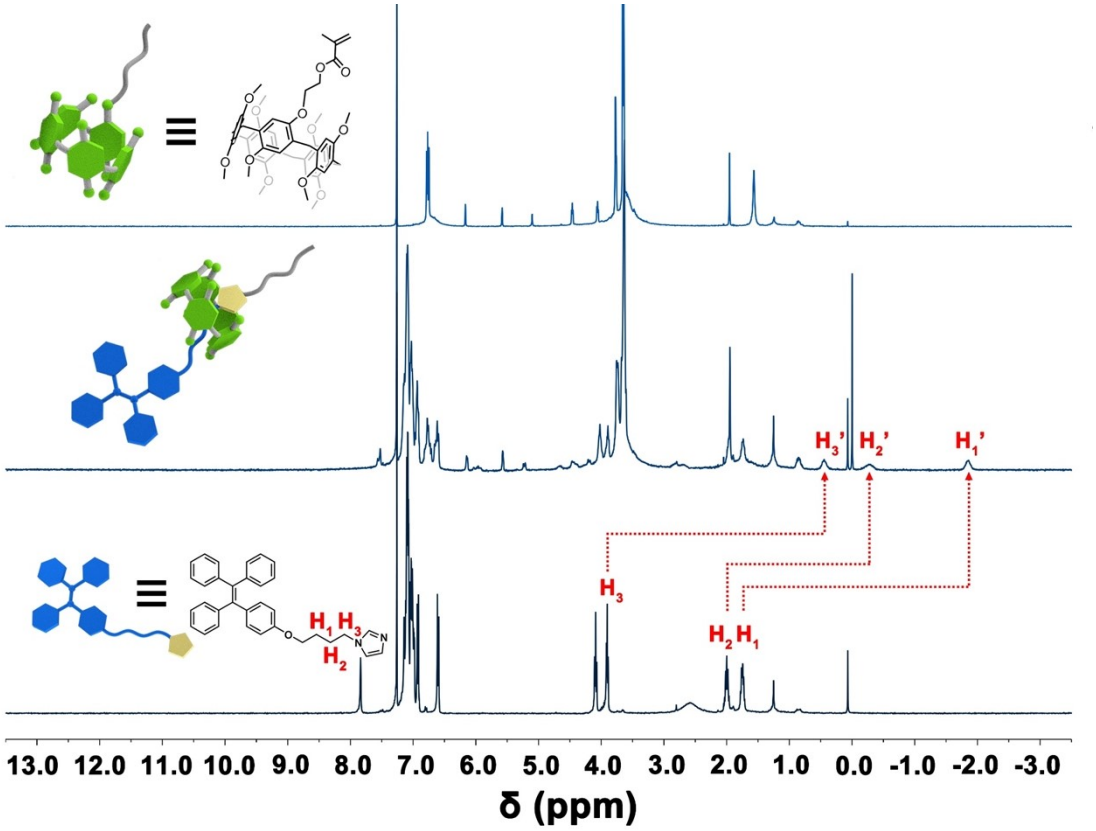

Fig. S18. ^1H NMR (600 MHz, 298 K, $CDCl_3$) spectra of (i) MMAP[5]A (5×10^{-3} M), (ii) the mixture of MMAP[5]A (5×10^{-3} M), TPE-Im (5×10^{-3} M), (iii) TPE-Im (5×10^{-3} M).

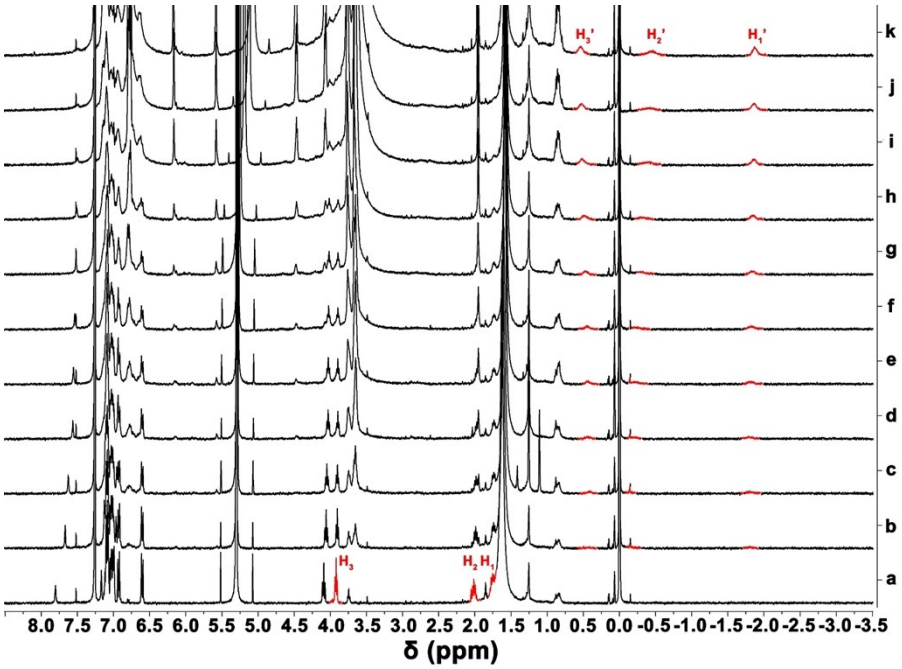

Fig. S19. ^{1}H NMR spectra of TPE-Im (1×10^{-3} M) upon addition of MMAP[5]A with various concentration (from bottom to top: 0, 0.2, 0.4, 0.6, 0.8, 1.0, 1.5, 2.0, 4.0, 6.0, 10.0 $\times10^{-3}$ M).

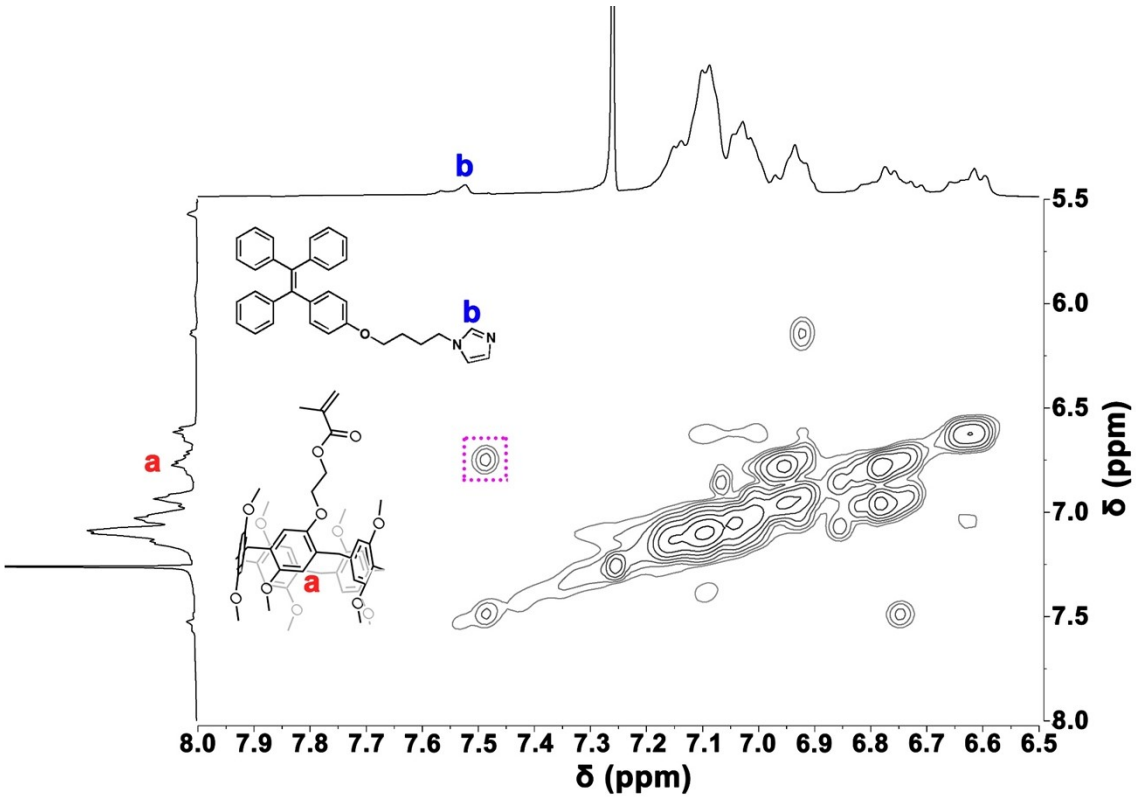

Fig. S20. Partial 2D NOESY spectrum (600 MHz, $CDCl_3$, 298 K) of TPE-Im ⊂ MMAP[5]A, [MMAP[5]A] = 3×10^{-2} M, [TPE-Im] = 3×10^{-2} M.

It was suggested that a sharp chemical shift occured, even if the addition of MMAP[5]A was trace amount. Furthermore, the observation of complexed and uncomplexed signals of alkyl groups belonging to TPE-Im in both Figure S18 and S19 certified the slow exchange rate on NMR time scale.

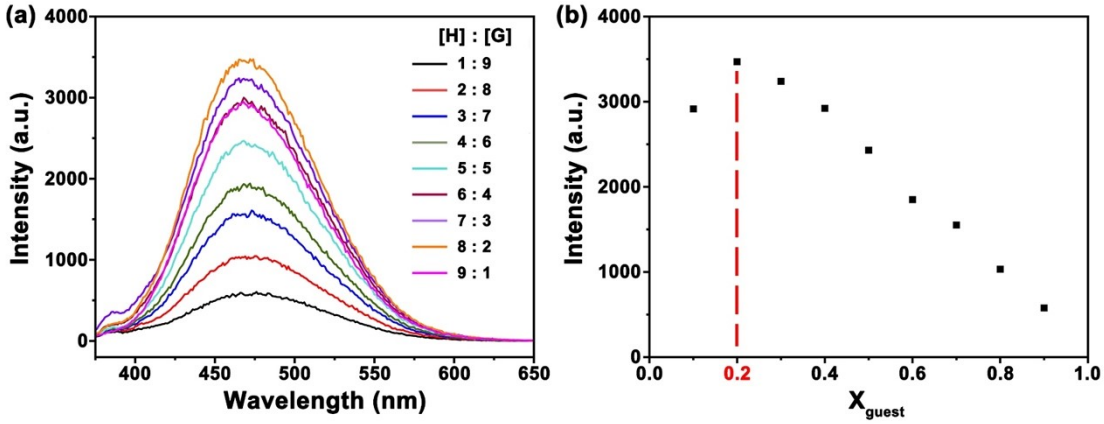

Fig. S21. Job's plot between PH1 and TPE-$(Im)_4$ collected by plotting fluorescence emission intensity appeared at 465 nm against the change in the molar fraction of TPE-$(Im)_4$ (X_{guest}). H represent pillar[5]arene unit; G represent TPE-$(Im)_4$, [pillar[5]arene unit] + [TPE-$(Im)_4$] = 60 μM. The plot indicates a 4:1 binding ratio between pillar[5]arene unit and TPE-$(Im)_4$.

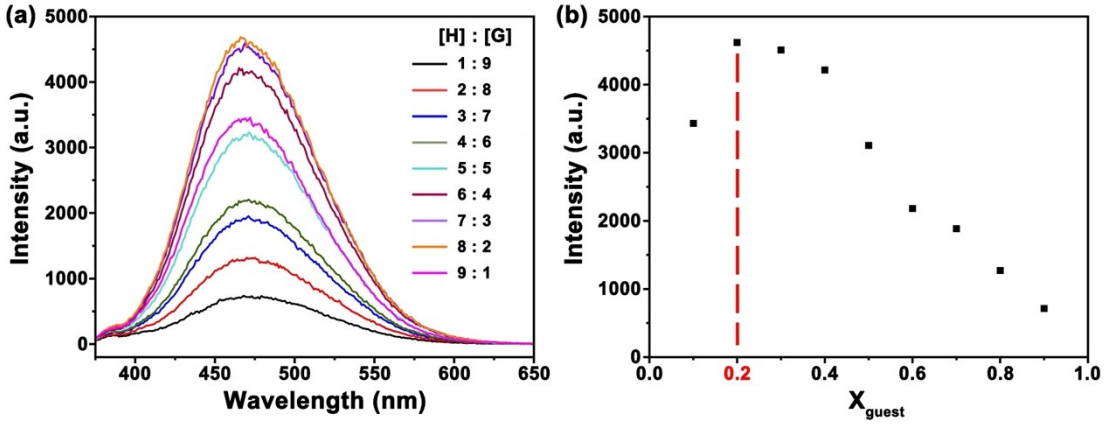

Fig. S22. Job's plot between PH2 and TPE-$(Im)_4$ collected by plotting fluorescence emission intensity appeared at 465 nm against the change in the molar fraction of TPE-$(Im)_4$ (X_{guest}). H represent pillar[5]arene unit; G represent TPE-$(Im)_4$, [pillar[5]arene unit] + [TPE-$(Im)_4$] = 60 μM. The plot indicates a 4:1 binding ratio between pillar[5]arene unit and TPE-$(Im)_4$.

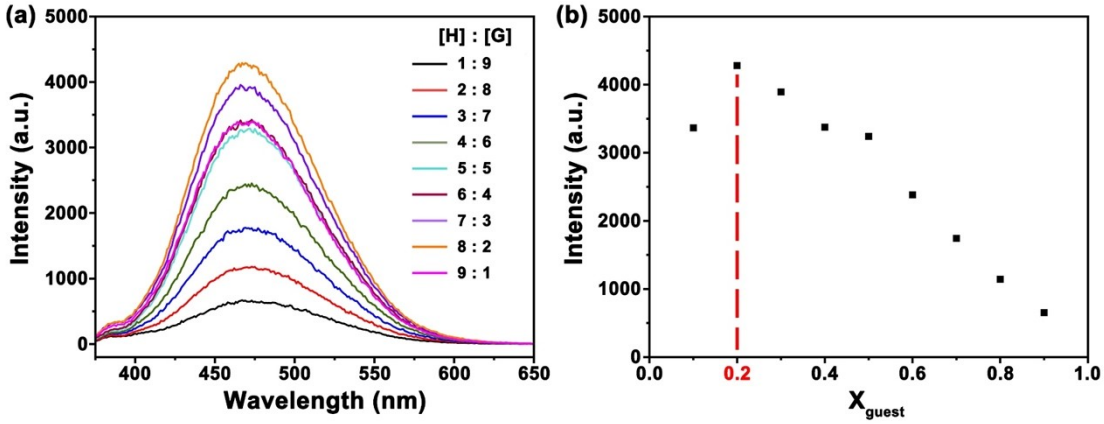

Fig. S23. Job's plot between PH3 and TPE-$(Im)_4$ collected by plotting fluorescence emission intensity appeared at 465 nm against the change in the molar fraction of TPE-$(Im)_4$ (X_{guest}). H represent pillar[5]arene unit; G represent TPE-$(Im)_4$, [pillar[5]arene unit] + [TPE-$(Im)_4$] = 60 μM. The plot indicates a 4:1 binding ratio between pillar[5]arene unit and TPE-$(Im)_4$.

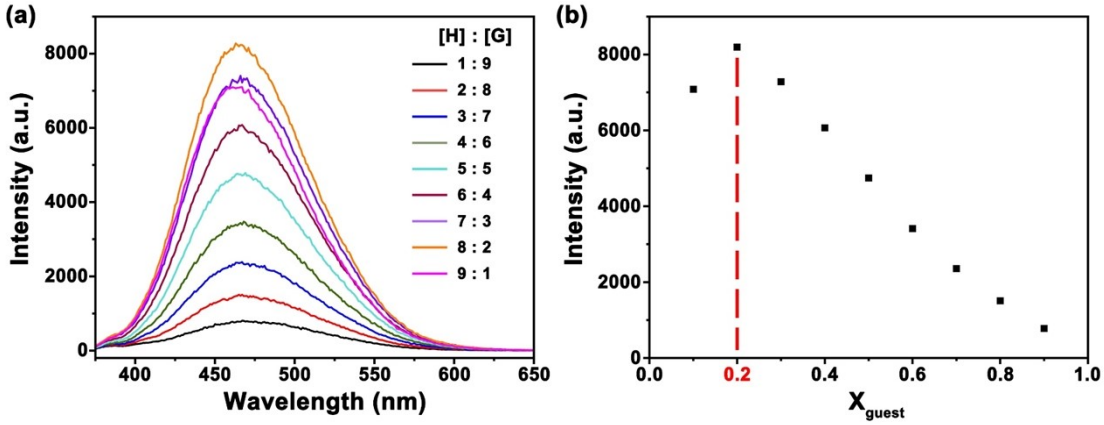

Fig. S24. Job's plot between PH4 and TPE-$(Im)_4$ collected by plotting fluorescence emission intensity appeared at 465 nm against the change in the molar fraction of TPE-$(Im)_4$ (X_{guest}). H represent pillar[5]arene unit; G represent TPE-$(Im)_4$, [pillar[5]arene unit] + [TPE-$(Im)_4$] = 60 μM. The plot indicates a 4:1 binding ratio between pillar[5]arene unit and TPE-$(Im)_4$.

3. Fluorescence enhancement of supramolecular networks

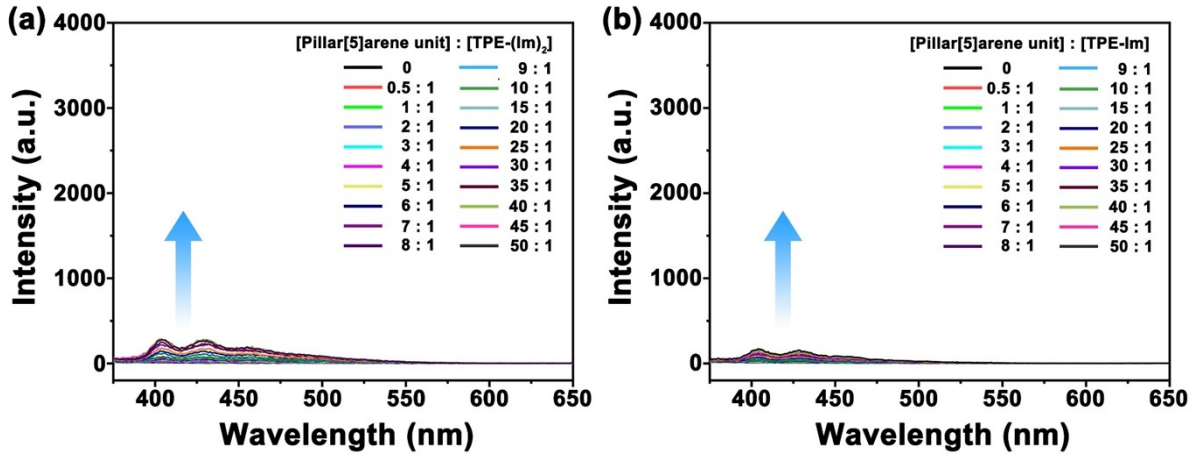

Fig. S25. Fluorescence emission spectra of (a) TPE-$(Im)_2$ ⊂ PH4, (b) TPE-Im ⊂ PH4 in THF solution. (λ_{ex} = 330 nm; [TPE-$(Im)_2$] = 1 × 10^{-6} M, [TPE-Im] = 1 × 10^{-6} M, [pillar[5]arene unit] = 0, 0.5, 1, 2, 3, 4, 5, 6, 7, 8, 9, 10, 15, 20, 25, 30, 35, 40, 45, 50 × 10^{-6} M).

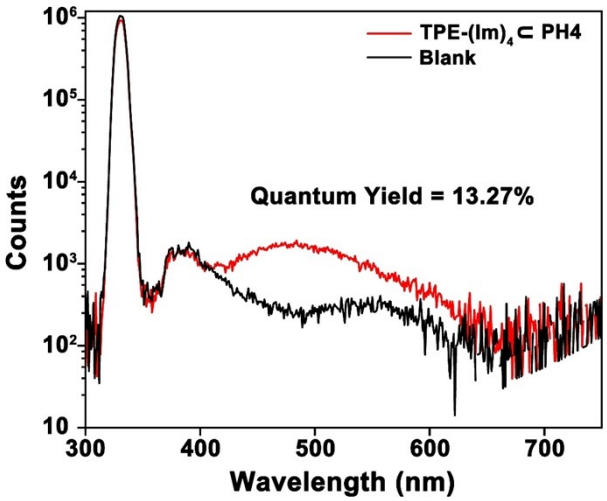

Fig. S26. Absolute fluorescence quantum yield of TPE-$(Im)_4$ ⊂ PH4 in THF solution. Experimental conditions: λ_{ex} = 330 nm; [pillar[5]arene unit] = 10 μM; [TPE-$(Im)_4$] = 1 μM; 25 °C.

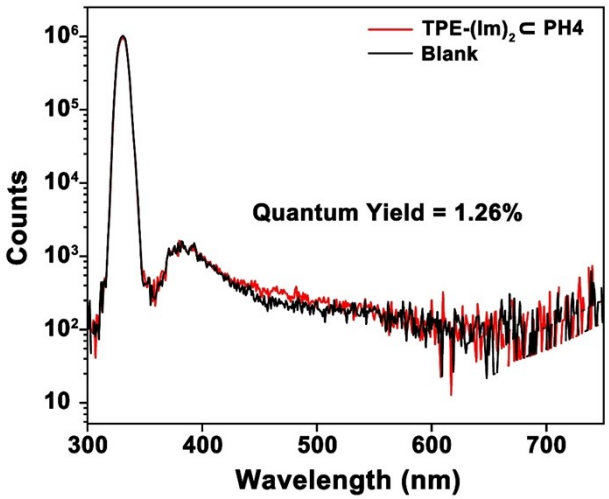

Fig. S27. Absolute fluorescence quantum yield of TPE-$(Im)_2$ ⊂ PH4 in THF solution. Experimental conditions: λ_{ex} = 330 nm; [pillar[5]arene unit] = 10 μM; [TPE-$(Im)_2$] = 1 μM; 25 °C.

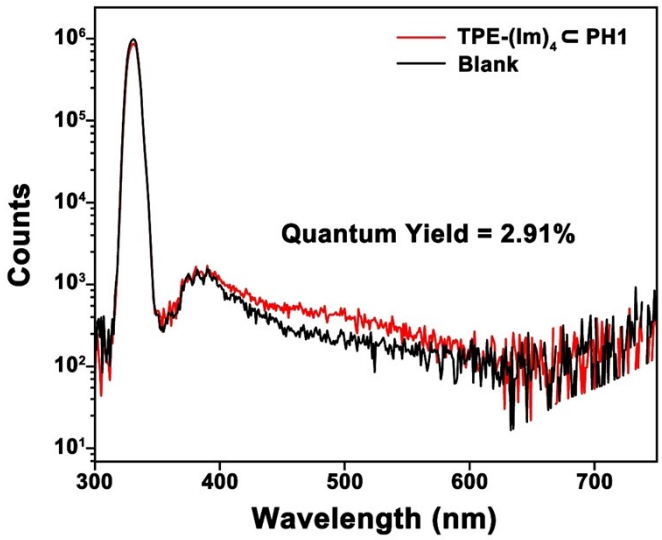

Fig. S28. Absolute fluorescence quantum yield of TPE-$(Im)_4$ ⊂ PH1 in THF solution. Experimental conditions: λ_{ex} = 330 nm; [pillar[5]arene unit] = 10 μM; [TPE-$(Im)_4$] = 1 μM; 25 °C.

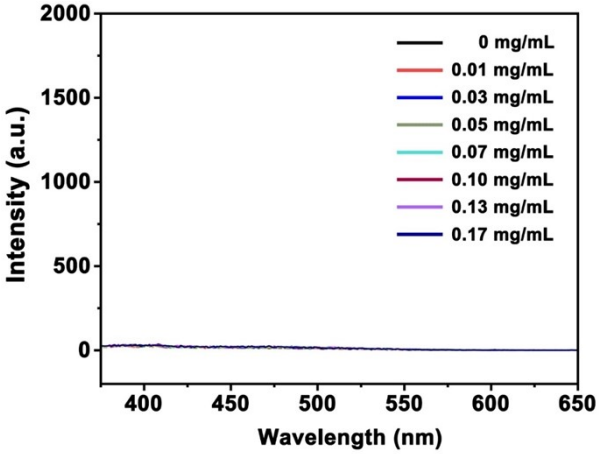

Fig. S29. Fluorescence intensities of TPE-$(Im)_4$ upon addition of P-c with different concentration in THF. The weight concentration of P-c was equal to PH2 by calculation.

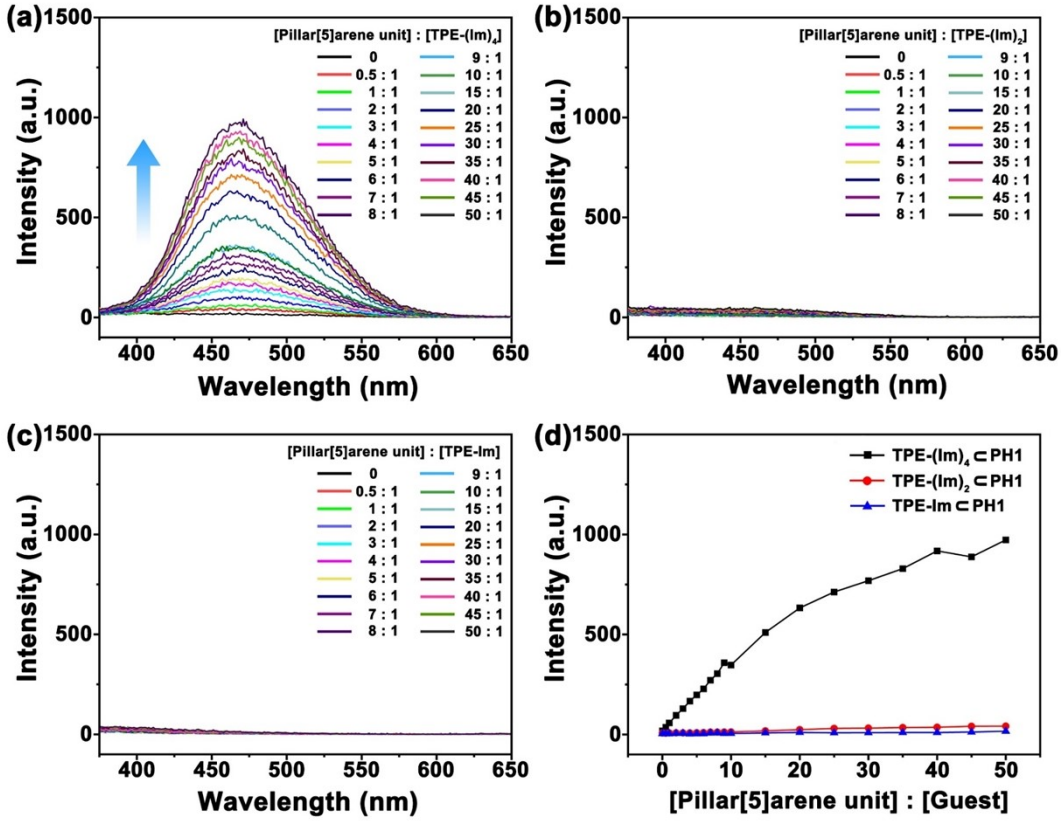

Fig. S30. Fluorescence emission spectra of (a) TPE-$(Im)_4$ ⊂ PH1, (b) TPE-$(Im)_2$ ⊂ PH1 and (c) TPE-Im ⊂ PH1 in THF solution. (λ_{ex} = 330 nm; 25 °C; [TPE-$(Im)_4$] = 1 × 10^{-6} M, [TPE-$(Im)_2$] = 1 × 10^{-6} M, [TPE-Im] = 1 × 10^{-6} M, [pillar[5]arene unit] = 0, 0.5, 1, 2, 3, 4, 5, 6, 7, 8, 9, 10, 15, 20, 25, 30, 35, 40, 45, 50 × 10^{-6} M). (d) Line chart of fluorescence emission intensities of

TPE-$(Im)_4$ ⊂ PH1 (black line), TPE-$(Im)_2$ ⊂ PH1 (red line) and TPE-Im ⊂ PH1 (blue line) appeared at 465 nm with different ratio of pillar[5]arene units to guest molecules.

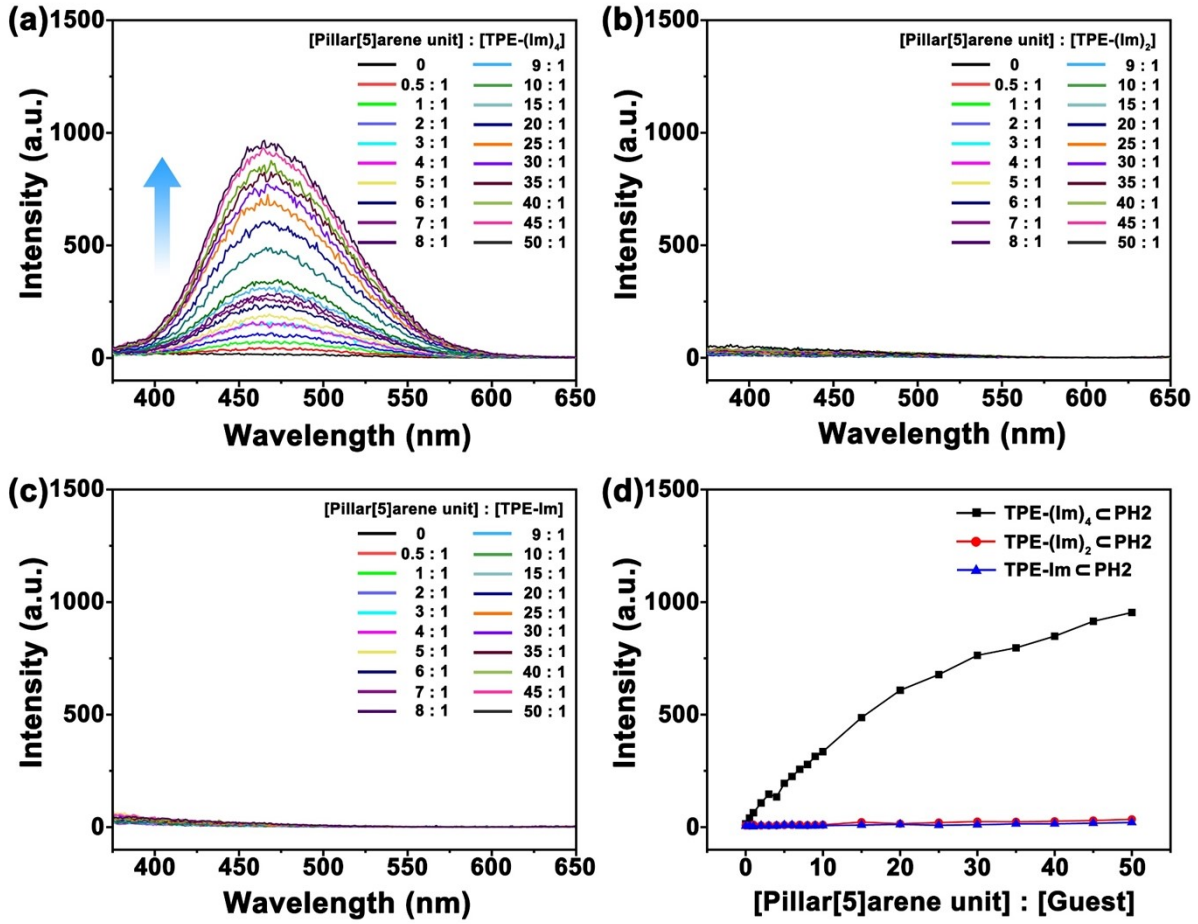

Fig. S31. Fluorescence emission spectra of (a) TPE-$(Im)_4$ ⊂ PH2, (b) TPE-$(Im)_2$ ⊂ PH2 and (c) TPE-Im ⊂ PH2 in THF solution. (λ_{ex} = 330 nm; 25 °C; [TPE-$(Im)_4$] = 1 × 10^{-6} M, [TPE-$(Im)_2$] = 1 × 10^{-6} M, [TPE-Im] = 1 × 10^{-6} M, [pillar[5]arene unit] = 0, 0.5, 1, 2, 3, 4, 5, 6, 7, 8, 9, 10, 15, 20, 25, 30, 35, 40, 45, 50 × 10^{-6} M). (d) Line chart of fluorescence emission intensities of TPE-$(Im)_4$ ⊂ PH2 (black line), TPE-$(Im)_2$ ⊂ PH2 (red line) and TPE-Im ⊂ PH2 (blue line) appeared at 465 nm with different ratio of pillar[5]arene units and guest molecules.

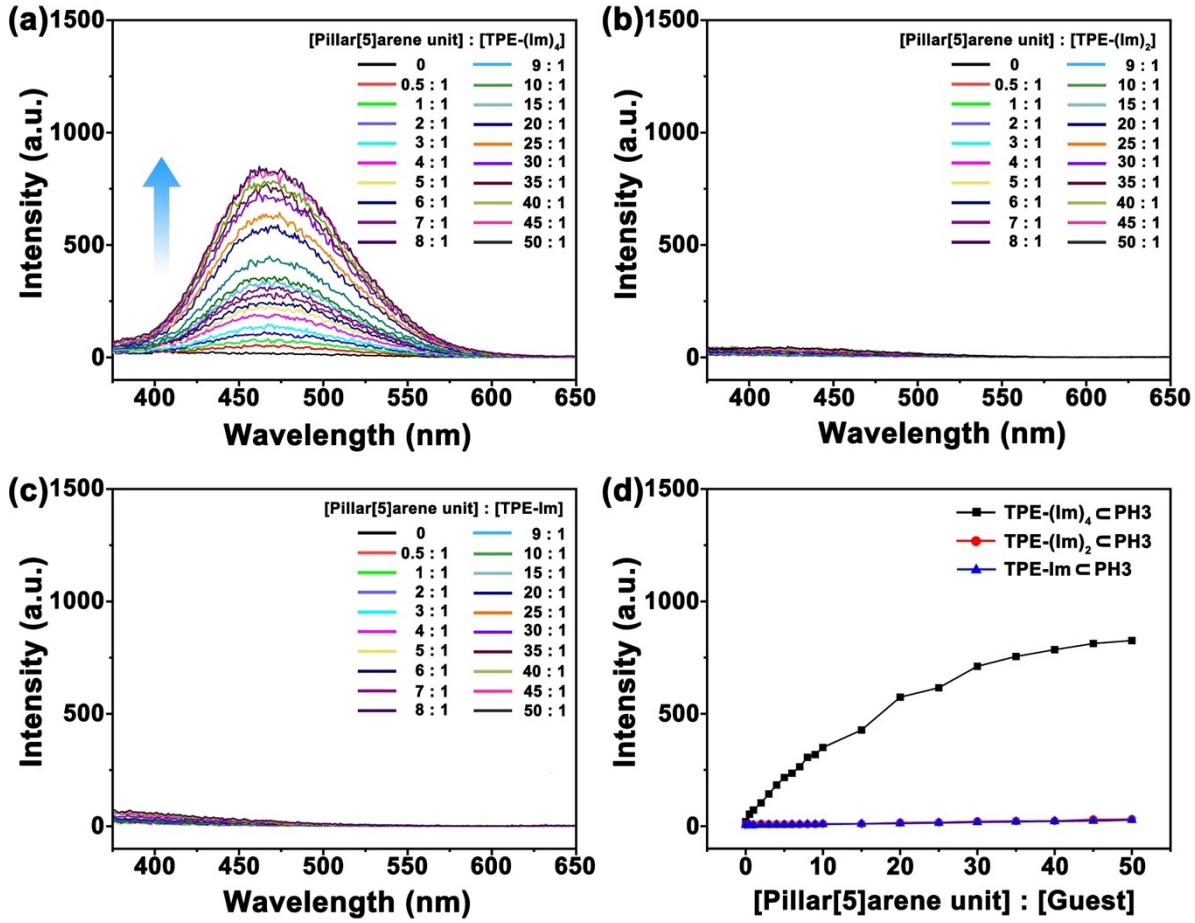

Fig. S32. Fluorescence emission spectra of (a) TPE-$(Im)_4$ ⊂ PH3, (b) TPE-$(Im)_2$ ⊂ PH3 and (c) TPE-Im ⊂ PH3 in THF solution. (λ_{ex} = 330 nm; 25 °C; [TPE-$(Im)_4$] = 1 × 10^{-6} M, [TPE-$(Im)_2$] = 1 × 10^{-6} M, [TPE-Im] = 1 × 10^{-6} M, [pillar[5]arene unit] = 0, 0.5, 1, 2, 3, 4, 5, 6, 7, 8, 9, 10, 15, 20, 25, 30, 35, 40, 45, 50 × 10^{-6} M). (d) Line chart of fluorescence emission intensities of TPE-$(Im)_4$ ⊂ PH3 (black line), TPE-$(Im)_2$ ⊂ PH3 (red line) and TPE-Im ⊂ PH3 (blue line) appeared at 465 nm with different ratio of pillar[5]arene units and guest molecules.

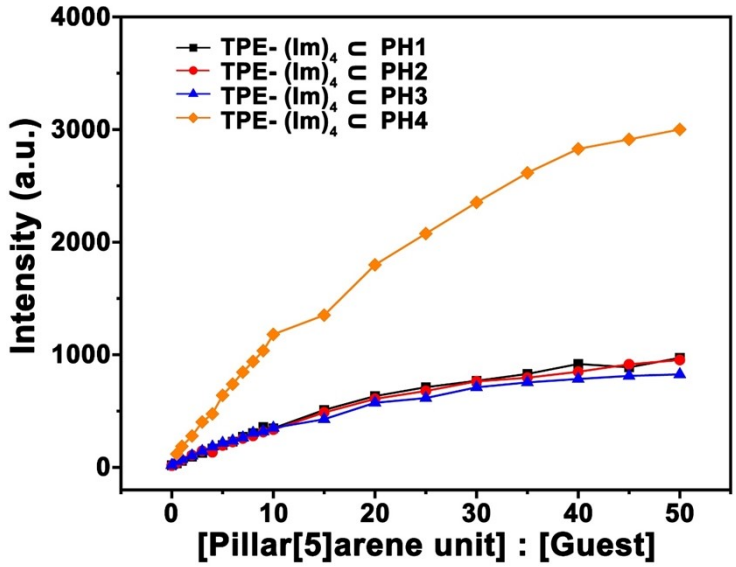

Fig. S33. (a) Fluorescence intensities of TPE-$(Im)_4$ ⊂ PH1 (black line), TPE-$(Im)_4$ ⊂ PH2 (red line), TPE-$(Im)_4$ ⊂ PH3 (blue line) and TPE-$(Im)_4$ ⊂ PH4 (orange line) appeared at 465 nm.

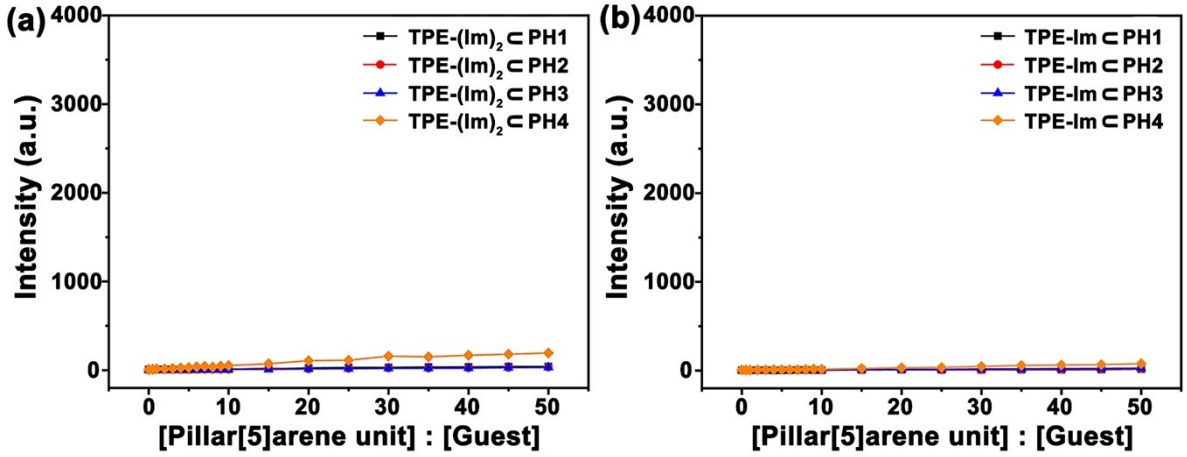

Fig. S34. (a) Fluorescence intensities of TPE-$(Im)_2$ ⊂ PH1 (black line), TPE-$(Im)_2$ ⊂ PH2 (red line), TPE-$(Im)_2$ ⊂ PH3 (blue line) and TPE-$(Im)_2$ ⊂ PH4 (orange line) at 465 nm. (b) Fluorescence intensities of TPE-Im ⊂ PH1 (black line), TPE-Im ⊂ PH2 (red line), TPE-Im ⊂ PH3 (blue line) and TPE-Im ⊂ PH4 (orange line) appeared at 465 nm.

In regard to line chart of emission intensities of SAIEE systems in THF regulated by different length of hydrophilic chains as depicted in Fig. S33 and S34, these results showed that SAIEE systems based on PH1, PH2 and PH3 exhibited similar emission intensities, indicating that the molecular weight and/or length of hydrophilic chains hardly affect the optical performance. In particular, the density of macrocycle and number of guest moiety exhibited

relatively large effect on their fluorescence emission intensities, which could be concluded from the abovementioned data.

4. Stimuli-responsive behavior

Due to the reversible assembly endowed by host-guest interactions, supramolecular networks formed by TPE-$(Im)_4$ ⊂ PH4 in THF solution exhibited stimuli-responsive behavior with addition of competitive agents and temperature variation. Upon addition of competitive agent adiponitrile that exhibited stronger binding affinity towards pillar[5]arene cavities, the supramolecular networks were broken, resulting in the quench of fluorescence (Fig. S35). Furthermore, the emission of supramolecular networks were also quenched by elevated temperature, and the fluorescence could be recorved when cooled down to room temperature for at least 7 cycles which was ascribed to the reversible assembly (Fig. S36 and S37).

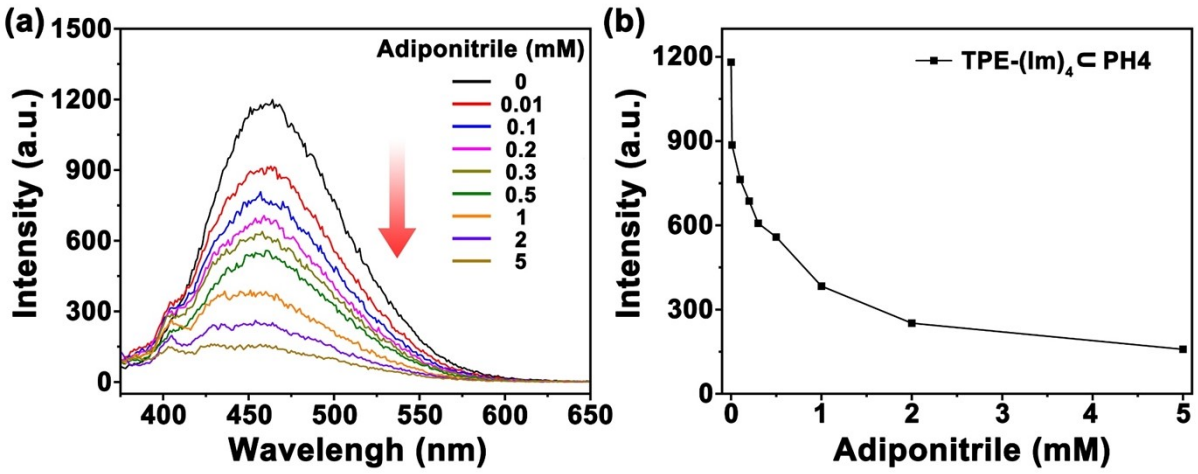

Fig. S35. (a) Fluorescence emission spectra of TPE-$(Im)_4$ ⊂ PH4 in THF solution upon addition of adiponitrile with different concentration (λ_{ex} = 330 nm; 25 °C; [TPE-$(Im)_4$] = 1 × 10^{-6} M, [adiponitrile] = 0, 0.01, 0.1, 0.2, 0.3, 0.5, 1, 2, 5 × 10^{-3} M , [pillar[5]arene unit] = 1 × 10^{-5} M). (b) Emission intensities of TPE-$(Im)_4$ ⊂ PH4 appeared at 465 nm with various concentration of adiponitrile.

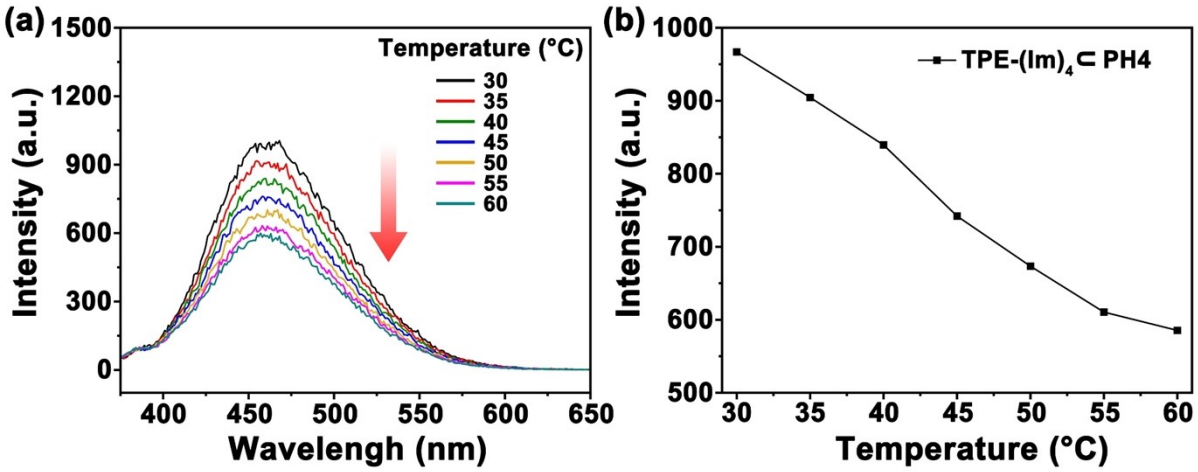

Fig. S36. (a) Fluorescence emission spectra of TPE-$(Im)_4$ ⊂ PH4 in THF solution with elevated temperature. (b) Line chart of emission intensities of TPE-$(Im)_4$ ⊂ PH4 appeared at 465 nm with temperature variation. Experimental conditions: λ_{ex} = 330 nm; [pillar[5]arene unit] = 10 μM; [TPE-$(Im)_4$] = 1 μM.

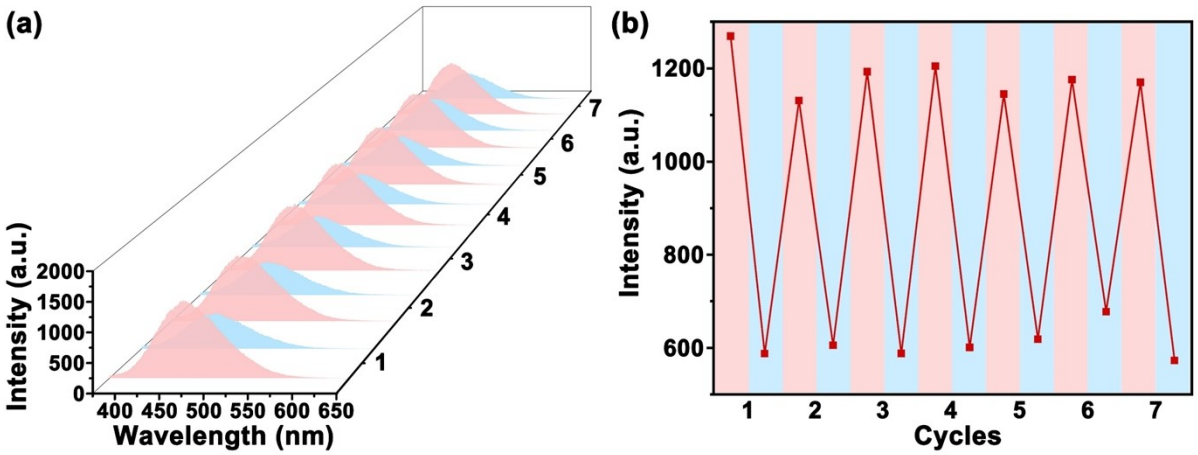

Fig. S37. (a) Fluorescence emission spectra of TPE-$(Im)_4$ ⊂ PH4 in seven thermal cycles, 30 °C (red), 60 °C (blue); (b) Line chart of emission intensities of TPE-$(Im)_4$ ⊂ PH4 in seven thermal cycles appeared at 465 nm. Experimental conditions: λ_{ex} = 330 nm; [pillar[5]arene unit] = 10 μM; [TPE-$(Im)_4$] = 1 μM.

5. Fluorescence enhancement of supramolecular assembly

It is well known that the morphology of self-assembly was largely depended on the amphipathy of macromolecules, as a result, we designed three types of block polymer hosts to

discuss the effect of morphology on optical performance. Surprsingly, the emission intensities of TPE-$(Im)_4$ ⊂ PH1, TPE-$(Im)_4$ ⊂ PH2 and TPE-$(Im)_4$ ⊂ PH3 were comparable while all three SAIEE systems exhibited contineously increased emission intensity upon addition of water in mixture solution (Fig. S41-S43). Furthermore, the optical performance of TPE-$(Im)_4$ ⊂ PH4 with double density of pillar[5]arene unit was almost identical to the abovementioned three polymer hosts (Fig. S44), which was opposite to those in THF solution. From the line chart of TPE-$(Im)_4$ and TPE-$(Im)_4$ & P-c in THF/H_2O mixed solvent with different f_w (Fig. S47), we could draw a conclusion that the hydrophobic interactions of amphiphilic polymer P-c was benificial to the emission enhancemnet of chromophores due to the formation of nanoparticles. Surprisingly, the TPE-$(Im)_4$ ⊂ PH2 in mixture solution exhibited the maximum emission intensity due to the concurrence of host-guest interactions and hydrophobic assembly of macromolecules.

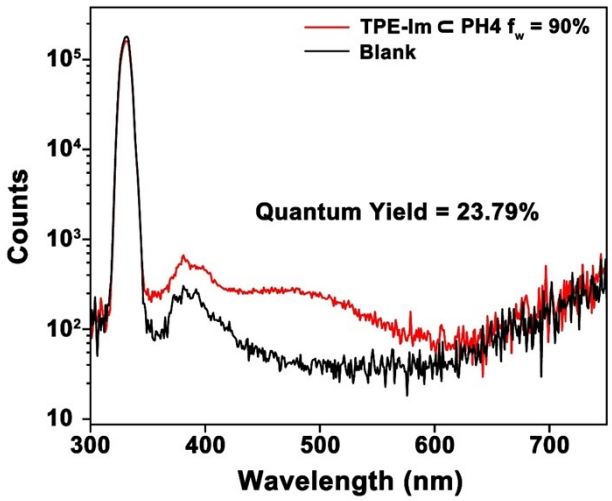

Fig. S38. Absolute fluorescence quantum yields of TPE-Im ⊂ PH4 in THF/H_2O mixed solution. Experimental conditions: λ_{ex} = 330 nm; [pillar[5]arene unit] = 10 μM; [TPE-$(Im)_4$] = 1 μM; f_w = 90%; 25 °C.

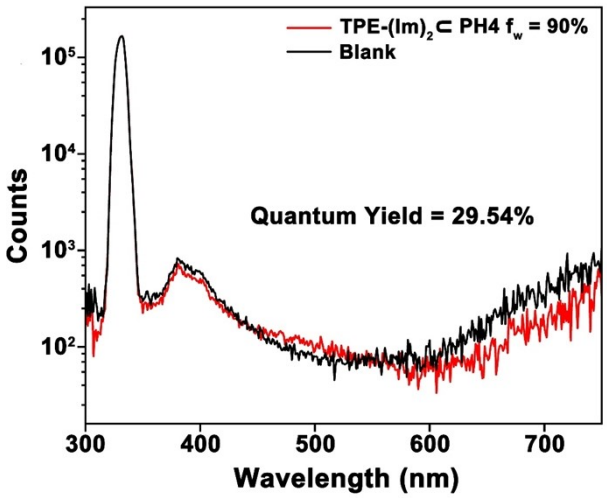

Fig. S39. Absolute fluorescence quantum yields of TPE-$(Im)_2$ ⊂ PH4 in THF/H_2O mixed solution. Experimental conditions: λ_{ex} = 330 nm; [pillar[5]arene unit] = 10 μM; [TPE-$(Im)_4$] = 1 μM; f_w = 90%; 25 °C.

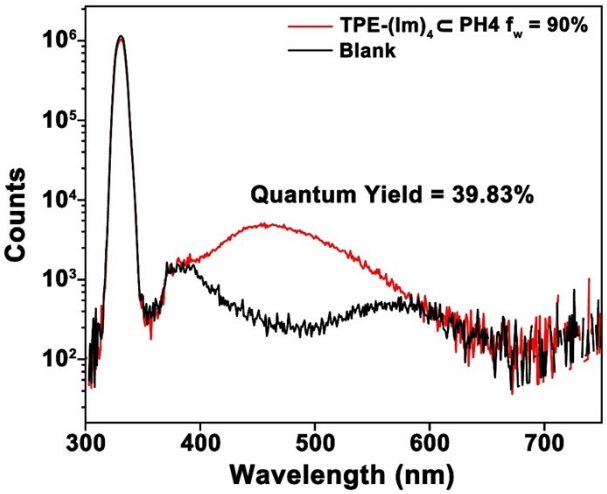

Fig. S40. Absolute fluorescence quantum yields of TPE-$(Im)_4$ ⊂ PH4 in THF/H_2O mixed solution. Experimental conditions: λ_{ex} = 330 nm; [pillar[5]arene unit] = 10 μM; [TPE-$(Im)_4$] = 1 μM; f_w = 90%; 25 °C.

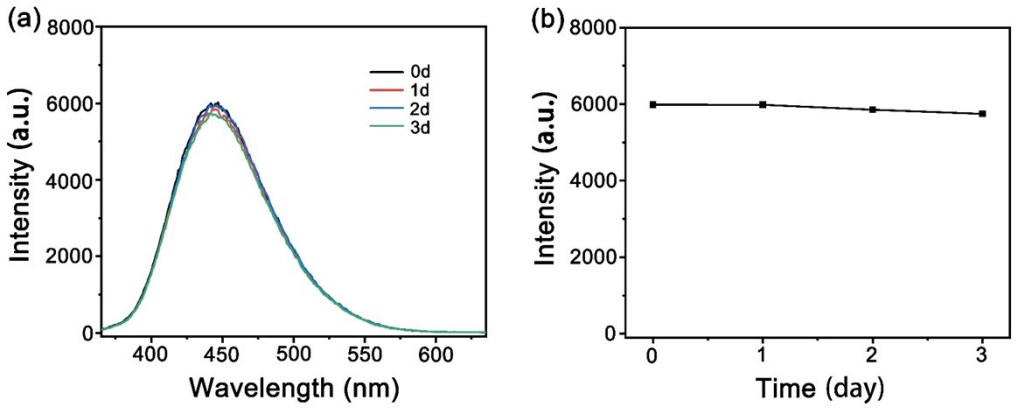

Fig. S41. (a) Fluorescence emission spectra and (b) line chart of TPE-$(Im)_4$ ⊂ PH1 in THF/H_2O mixed solvent with different days.

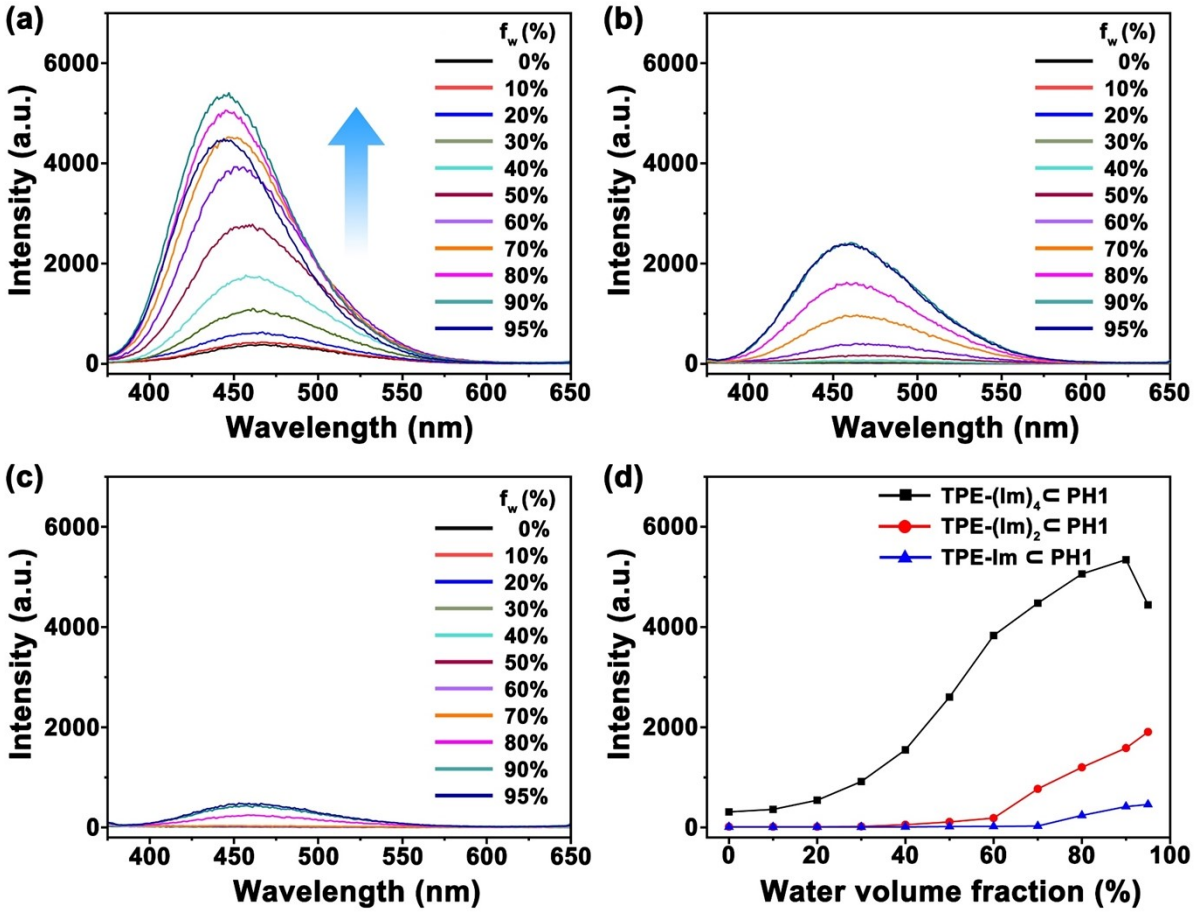

Fig. S42. Fluorescence emission spectra of (a) TPE-$(Im)_4$ ⊂ PH1, (b) TPE-$(Im)_2$ ⊂ PH1 and (c) TPE-Im ⊂ PH1 in THF/H_2O mixed solvent with various f_w. (d) Line chart of TPE-$(Im)_4$ ⊂ PH1 (black line), TPE-$(Im)_2$ ⊂ PH1 (red line) and TPE-Im ⊂ PH1 (blue line) in THF/H_2O mixed solvent with various f_w. Experimental conditions: λ_{ex} = 330 nm; slit widths: ex 5 nm, em 2.5

nm; [TPE-$(Im)_4$] = 1 × 10^{-6} M, [TPE-$(Im)_2$] = 1 × 10^{-6} M, [TPE-Im] = 1 × 10^{-6} M, [pillar[5]arene unit] = 1× 10^{-5} M; 25 °C.

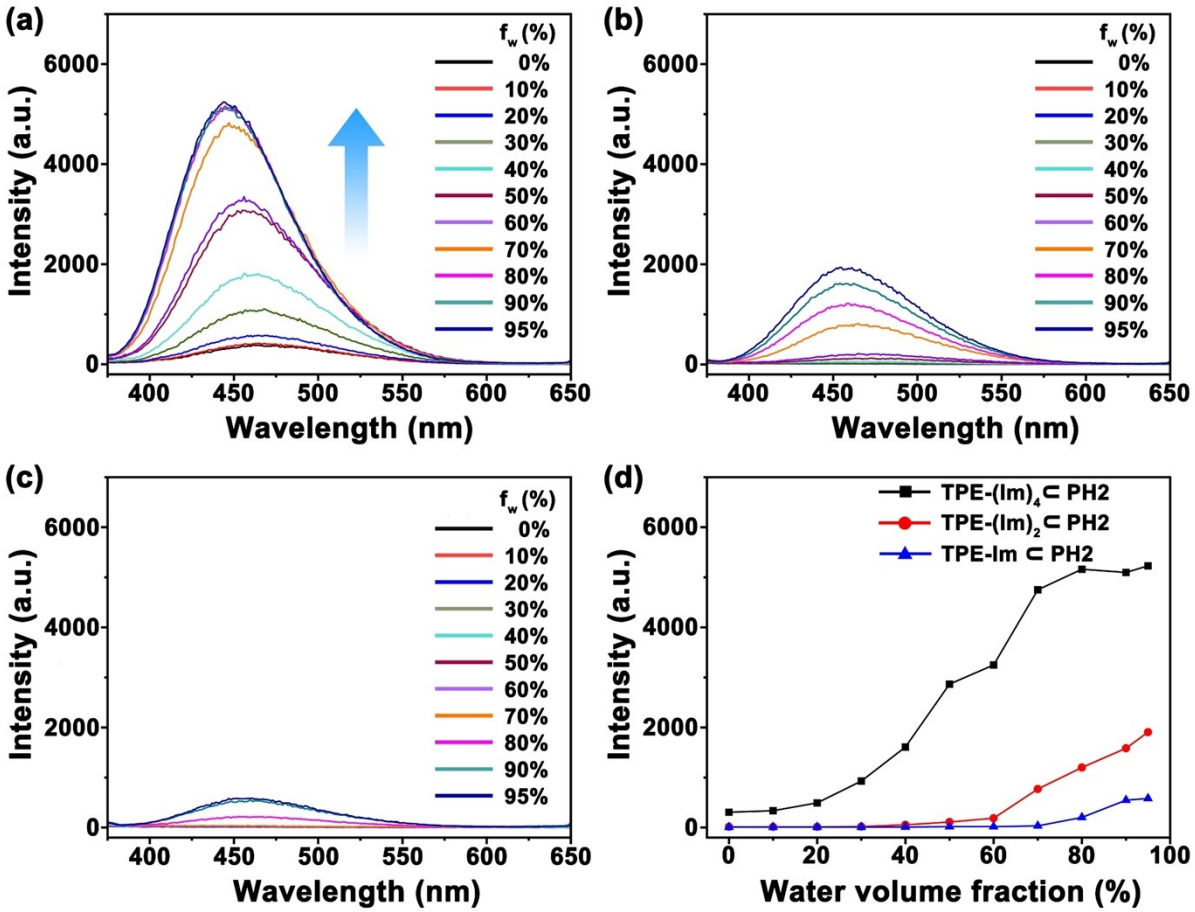

Fig. S43. Fluorescence emission spectra of (a) TPE-$(Im)_4$ ⊂ PH2, (b) TPE-$(Im)_2$ ⊂ PH2 and (c) TPE-Im ⊂ PH2 in THF/H_2O mixed solvent with various f_w. (d) Line chart of TPE-$(Im)_4$ ⊂ PH2 (black line), TPE-$(Im)_2$ ⊂ PH2 (red line) and TPE-Im ⊂ PH2 (blue line) in THF/H_2O mixed solvent with various f_w. **(**Experimental conditions: λ_{ex} = 330 nm; slit widths: ex 5 nm, em 2.5 nm; [TPE-$(Im)_4$] = 1 × 10^{-6} M, [TPE-$(Im)_2$] = 1 × 10^{-6} M, [TPE-Im] = 1 × 10^{-6} M, [pillar[5]arene unit] = 1× 10^{-5} M; 25 °C)

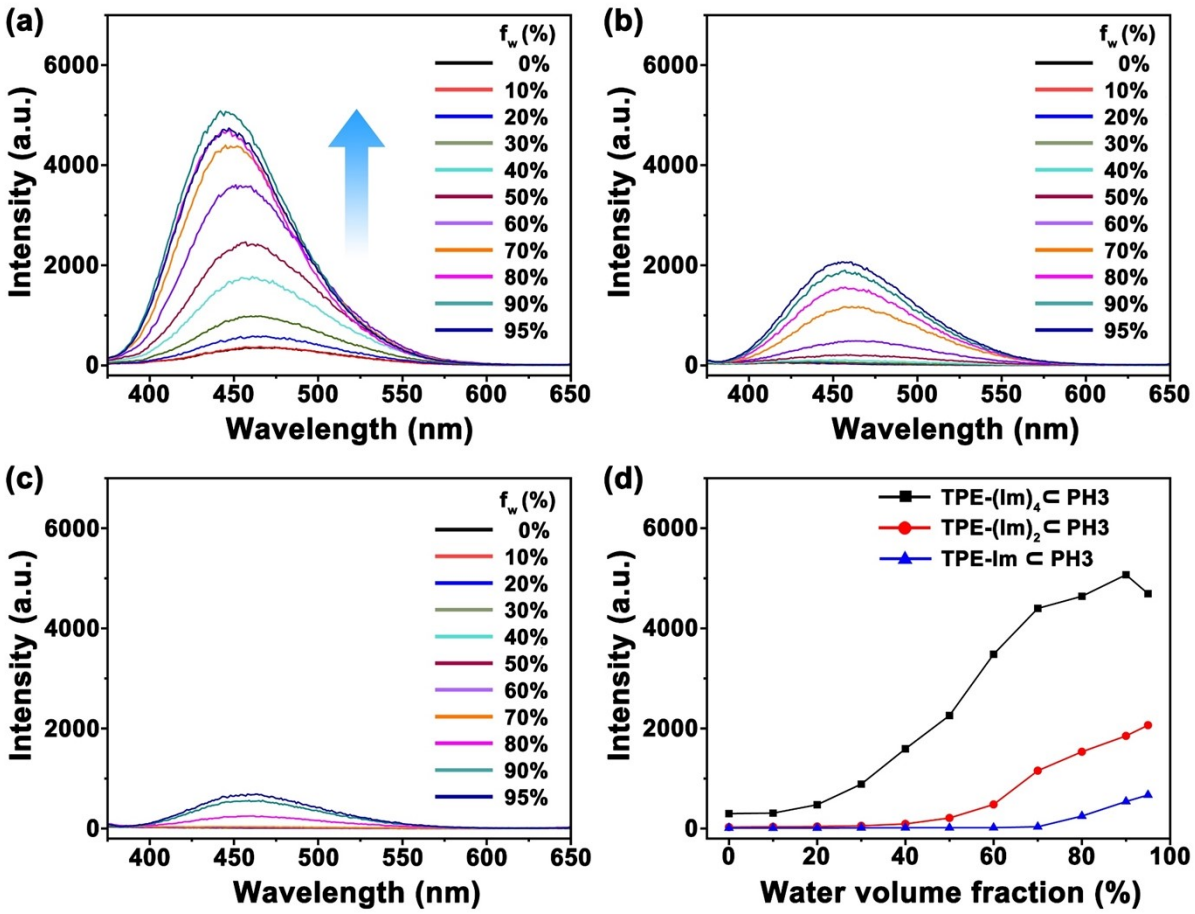

Fig. S44. Fluorescence emission spectra of (a) TPE-$(Im)_4$ ⊂ PH3, (b) TPE-$(Im)_2$ ⊂ PH3 and (c) TPE-Im ⊂ PH3 in THF/H_2O mixed solvent with various f_w. (d) Line chart of TPE-$(Im)_4$ ⊂ PH3 (black line), TPE-$(Im)_2$ ⊂ PH3 (red line) and TPE-Im ⊂ PH3 (blue line) in THF/H_2O mixed solvent with various f_w. (Experimental conditions: λ_{ex} = 330 nm; slit widths: ex 5 nm, em 2.5 nm; [TPE-$(Im)_4$] = 1 × 10^{-6} M, [TPE-$(Im)_2$] = 1 × 10^{-6} M, [TPE-Im] = 1 × 10^{-6} M, [pillar[5]arene unit] = 1× 10^{-5} M; 25 °C)

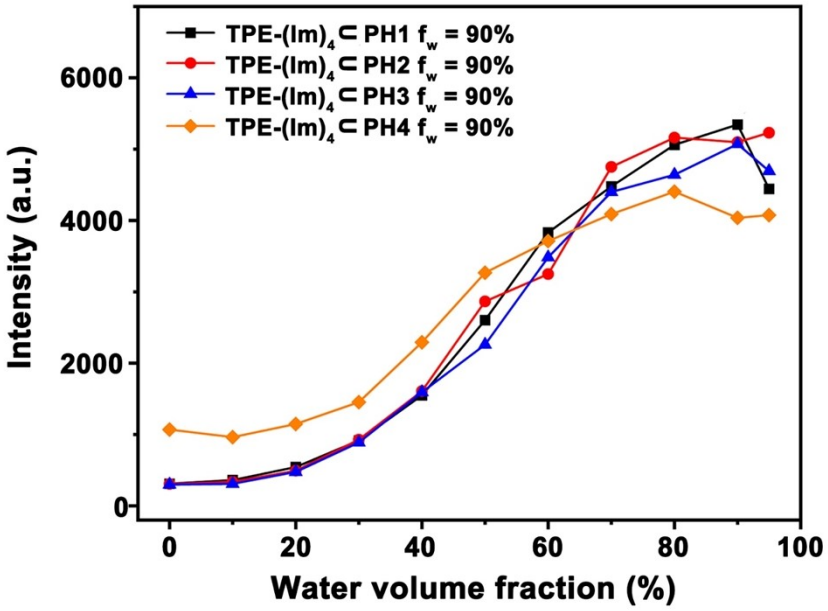

Fig. S45. Fluorescence emission intensities of TPE-$(Im)_4$ ⊂ PH1 (black line), TPE-$(Im)_4$ ⊂ PH2 (red line), TPE-$(Im)_4$ ⊂ PH3 (blue line) and TPE-$(Im)_4$ ⊂ PH4 (orange line) appeared at 445 nm in THF/H_2O mixed solvent with various f_w. **(**Experimental conditions: λ_{ex} = 330 nm; slit widths: ex 5 nm, em 2.5 nm; [TPE-$(Im)_4$] = 1 × 10^{-6} M, [pillar[5]arene unit] = 1× 10^{-5} M; 25 °C)

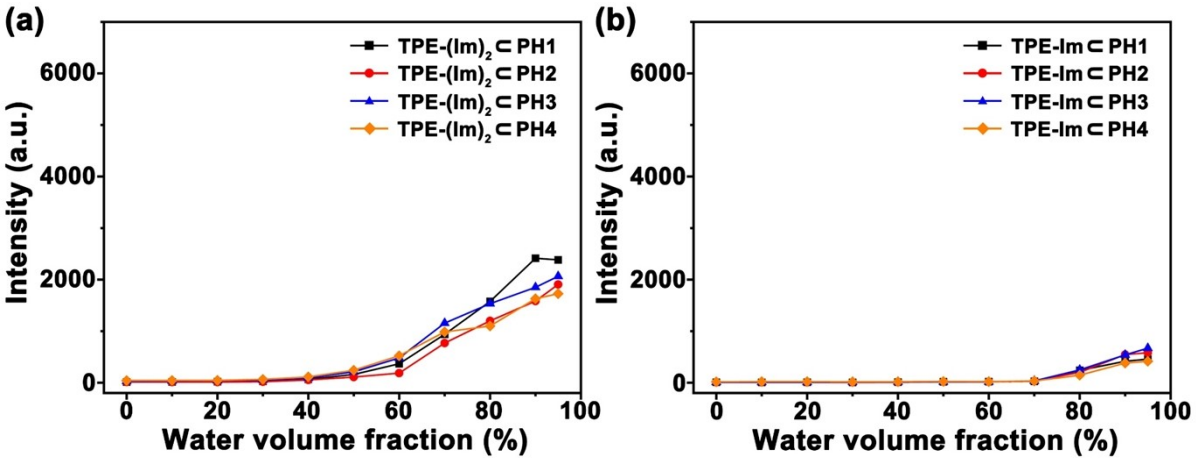

Fig. S46. (a) Fluorescence emission intensities of TPE-$(Im)_2$ ⊂ PH1 (black line), TPE-$(Im)_2$ ⊂ PH2 (red line), TPE-$(Im)_2$ ⊂ PH3 (blue line) and TPE-$(Im)_2$ ⊂ PH4 (orange line) appeared at 445 nm in THF/H_2O mixed solvent with various f_w. (b) Fluorescence intensities of TPE-Im ⊂ PH1 (black line), TPE-Im ⊂ PH2 (red line), TPE-Im ⊂ PH3 (blue line) and TPE-Im ⊂ PH4 (orange line) at 445 nm in THF/H_2O mixed solvent with various f_w. (Experimental conditions:

λ_{ex} = 330 nm; slit widths: ex 5 nm, em 2.5 nm; [TPE-$(Im)_2$] = 1 × 10^{-6} M, [TPE-Im] = 1 × 10^{-6} M, [pillar[5]arene unit] = 1× 10^{-5} M; 25 °C)

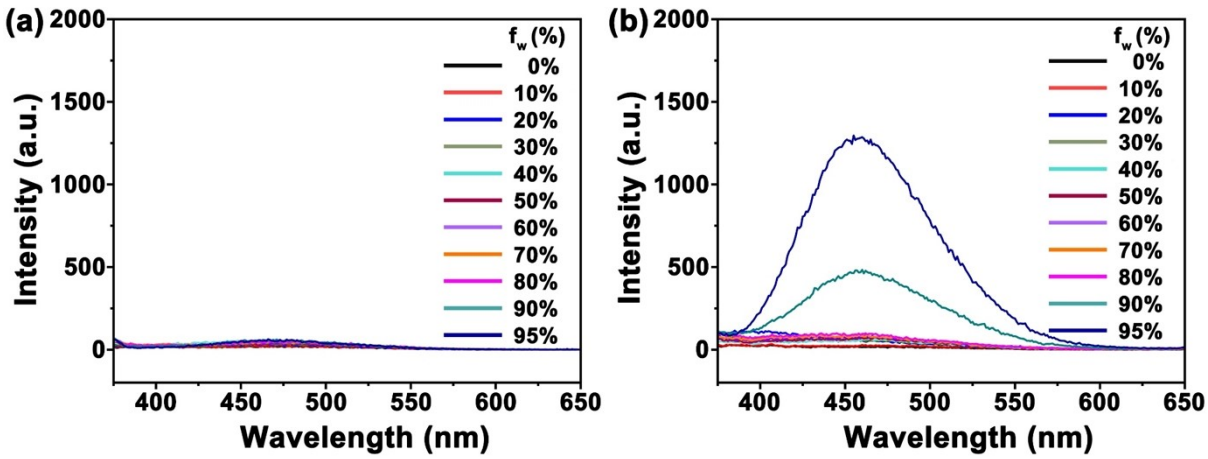

Fig. S47. Fluorescence emission intensities of (a) TPE-$(Im)_4$ and (b) TPE-$(Im)_4$ & P-c in THF/H_2O mixed solvent with various f_w. (Experimental conditions: λ_{ex} = 330 nm; slit widths: ex 5 nm, em 2.5 nm; [TPE-$(Im)_4$] = 1 × 10^{-6} M, $C_{(P\text{-}c)}$ = 0.03 mg/mL; 25 °C)

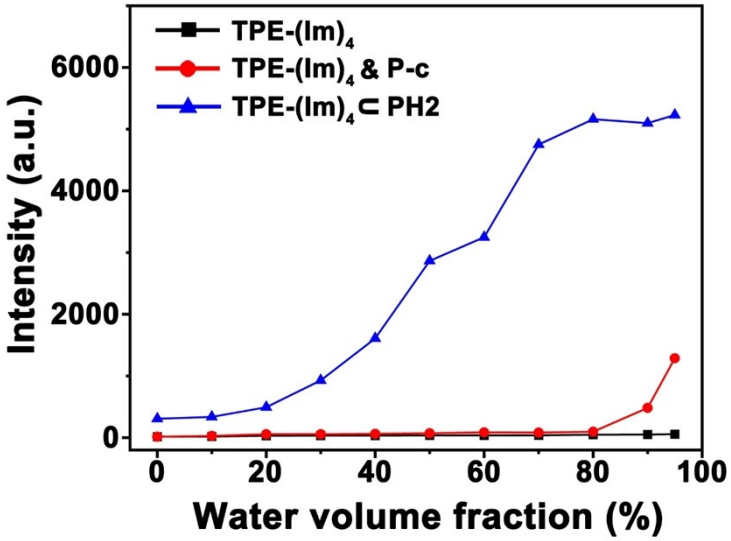

Fig. S48. Comparison of emission intensities appeared at 445 nm of TPE-$(Im)_4$ (black line), TPE-$(Im)_4$ ⊂ PH2 (blue line) and TPE-$(Im)_4$ & P-c (red line) in THF/H_2O mixed solvent with various f_w. As shown in Fig. S47, although the emission intensity of TPE-$(Im)_4$ & P-c was intensified upon addition of P-c, the emission intensity of TPE-$(Im)_4$ ⊂ PH2 was much higher than those of TPE-$(Im)_4$ & P-c, suggesting the crucial function of molecular recognition.

6. Characterization of morphology

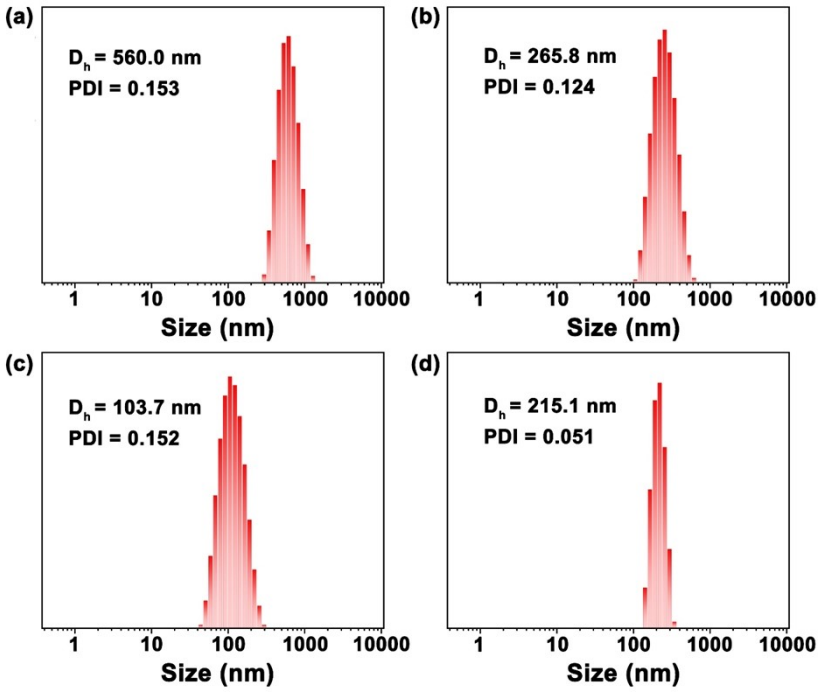

Fig. S49. Hydrodynamic sizes of (a) TPE-$(Im)_4$ ⊂ PH1; (b) TPE-$(Im)_4$ ⊂ PH2; (c) TPE-$(Im)_4$ ⊂ PH3 and (d) TPE-$(Im)_4$ ⊂ PH4 in THF/H_2O mixed solvent with f_w of 90%. (Experimental conditions: [TPE-$(Im)_4$] = 1×10^{-6} M, [pillar[5]arene unit] = 1×10^{-5} M)

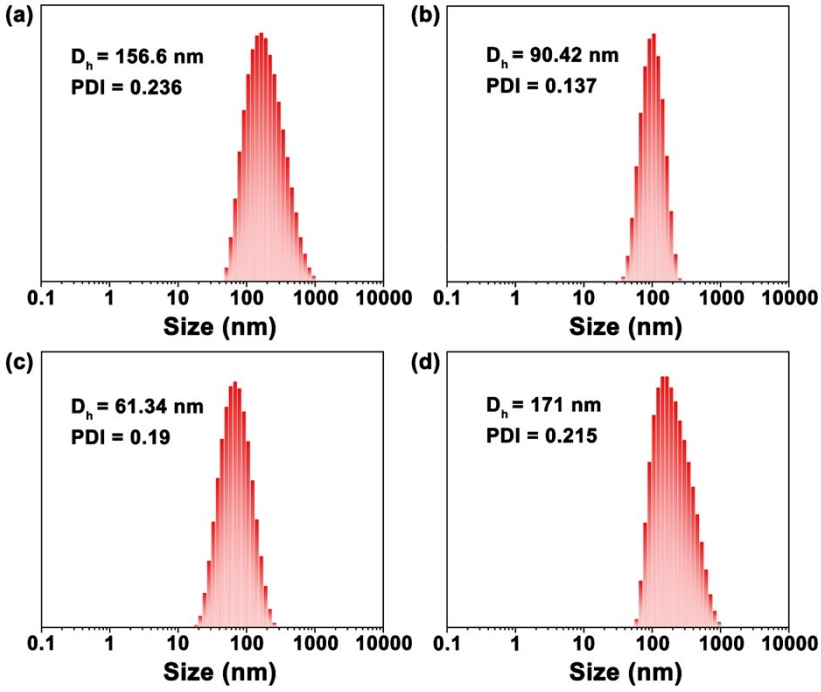

Fig. S50. Hydrodynamic sizes of (a) TPE-$(Im)_4$ ⊂ PH1; (b) TPE-$(Im)_4$ ⊂ PH2; (c) TPE-$(Im)_4$ ⊂ PH3 and (d) TPE-$(Im)_4$ ⊂ PH4 in aqueous solution. (Experimental conditions: [TPE-$(Im)_4$] = 1×10^{-6} M, [pillar[5]arene unit] = 1×10^{-5} M)

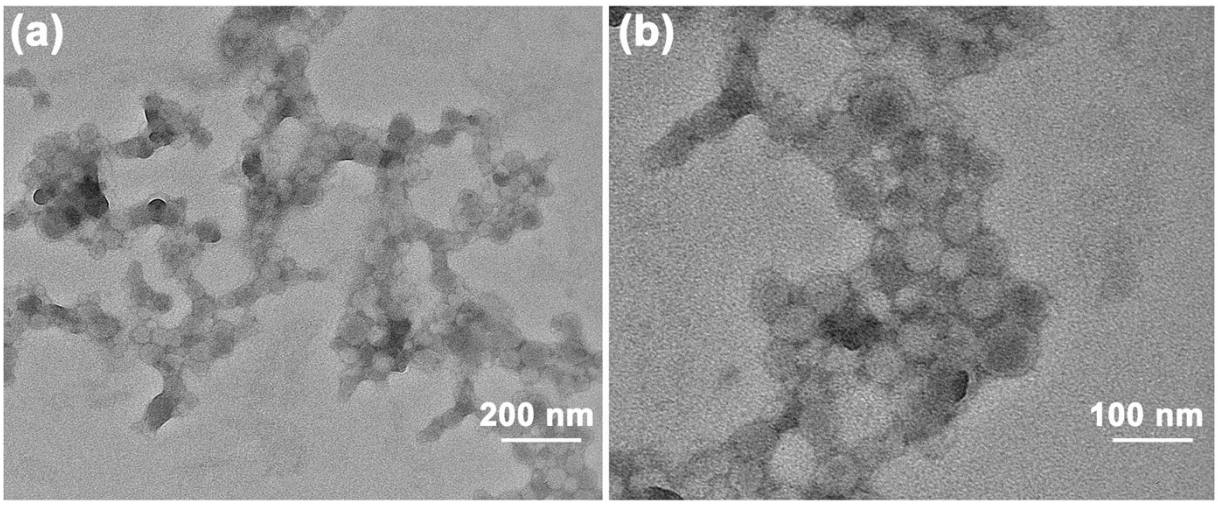

Fig. S51. TEM images of TPE-$(Im)_4$ ⊂ PH4 supramolecular vesicles after dialysis against water for 24 h. (Experimental conditions: [TPE-$(Im)_4$] = 1×10^{-6} M, [pillar[5]arene unit] = 1×10^{-5} M). The distinct boundary of supramolecular assembly suggested the vesicle structures of TPE-$(Im)_4$ ⊂ PH4 in aqueous solution, and their thickness were measured to be ca. 8 nm.

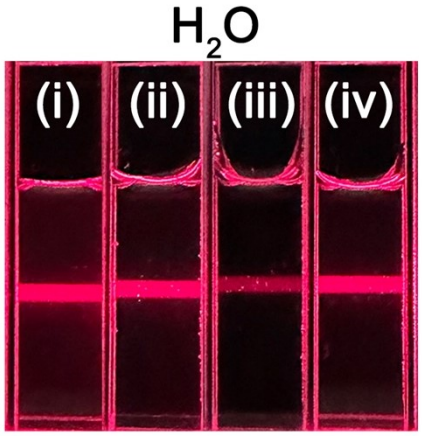

Fig. S52. Tyndell effect of (i) TPE-$(Im)_4$ ⊂ PH1, (ii) TPE-$(Im)_4$ ⊂ PH2, (iii) TPE-$(Im)_4$ ⊂ PH3 and (iv) TPE-$(Im)_4$ ⊂ PH4 in aqueous solution. (Experimental conditions: [TPE-$(Im)_4$] = 1×10^{-6} M, [pillar[5]arene unit] = 1×10^{-5} M). The observed tyndell effect suggested the formation of supramolecular assembly in aqueous solution.

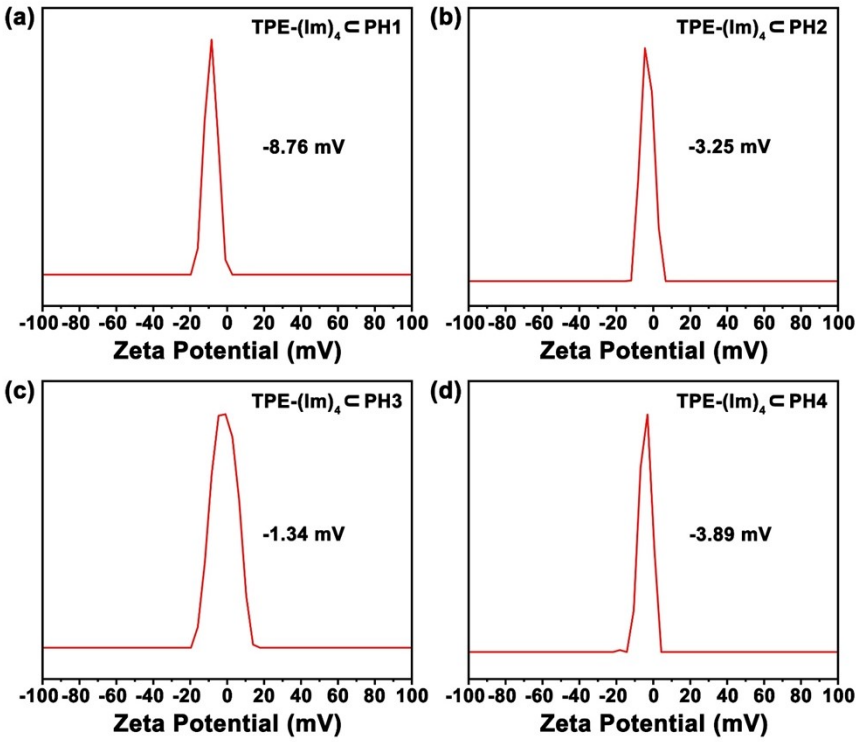

Fig. S53. Zeta potential of (a) TPE-$(Im)_4$ ⊂ PH1; (b) TPE-$(Im)_4$ ⊂ PH2; (c) TPE-$(Im)_4$ ⊂ PH3 and (d) TPE-$(Im)_4$ ⊂ PH4 in aqueous solution. (Experimental conditions: [TPE-$(Im)_4$] = 1×10^{-6} M, [pillar[5]arene unit] = 1×10^{-5} M)

The zeta potential of polymeric vesicles became electroneutrality upon lengthen the hydrophilic segments due to the supramolecular assembly was embedded by more $PEGMA_{300}$.

7. Fabrication of artificial light-harvesting systems

Calculation of energy transfer efficiency (Φ_{ET}):

Energy transfer efficiency was calculated by the following equation:

$$\Phi_{ET} = 1\text{-}(I_{DA,\,330}/I_{D,\,330})$$

$I_{DA,\,330}$ represent the emission intensity of TPE-$(Im)_4$ & DBT ⊂ PH4 appeared at 445 nm with different concentration of DBT under excitation at 330 nm; $I_{D,\,330}$ represent the emission intensity of TPE-$(Im)_4$ ⊂ PH4 appeared at 445 nm without DBT under excitation at 330 nm. The Φ_{ET} was depicted in Tables S1-S4 with different concentration of DBT in artificial light-harvesting systems.

Calculation of antenna effect (AE):

The antenna effect was calculated according to the following equation:

$$AE = (I_{DA,\,330}\text{-}I_{D,\,330})/I_{DA,\,445}$$

$I_{DA,\,330}$ represent the the fluorescence emission intensity at 545 nm of TPE-$(Im)_4$ & DBT ⊂ PH4 under excitation at 330 nm; $I_{D,\,330}$ represent the fluorescence emission intensity at 545 nm of TPE-$(Im)_4$ ⊂ PH4 under excitation at 330 nm; $I_{DA,\,450}$ represent the the fluorescence emission intensity at 545 nm of TPE-$(Im)_4$ & DBT ⊂ PH4 under excitation at 445 nm. The AE value was depicted in Tables S1-S4 with different concentration of DBT in artificial light-harvesting systems.

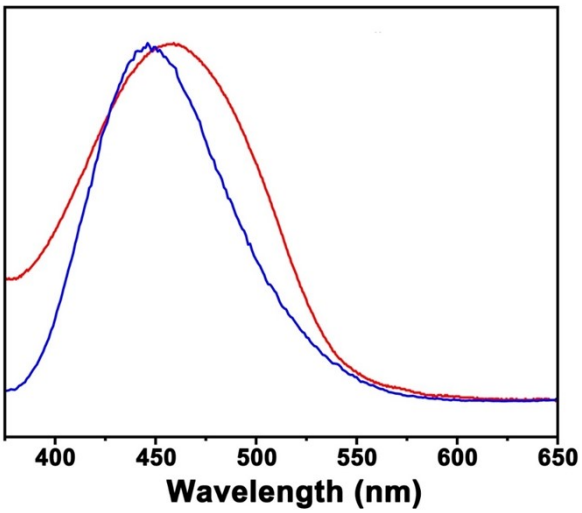

Fig. S54. The overlapped of normalized fluorescence emission spectrum of TPE-$(Im)_4$ ⊂ PH4 (blue line) and ultraviolet-visible spectrum of DBT (red line). Experimental conditions: λ_{ex} = 330 nm, f_w = 90%, [TPE-$(Im)_4$] = 1 × 10^{-6} M, [DBT] =3 × 10^{-5} M, [pillar[5]arene unit] = 1 × 10^{-5} M.

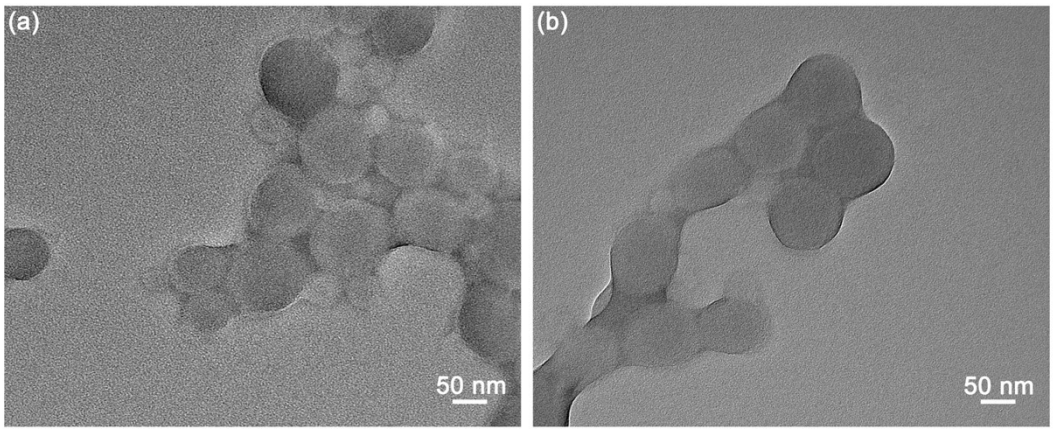

Fig. S55. TEM images of TPE-$(Im)_4$ & DBT ⊂ PH4 supramolecular polymer vesicles after dialysis against water for 24 h, [TPE-$(Im)_4$] = 1×10^{-6} M, [DBT] = 5×10^{-7} M, [pillar[5]arene unit] = 1×10^{-5} M.

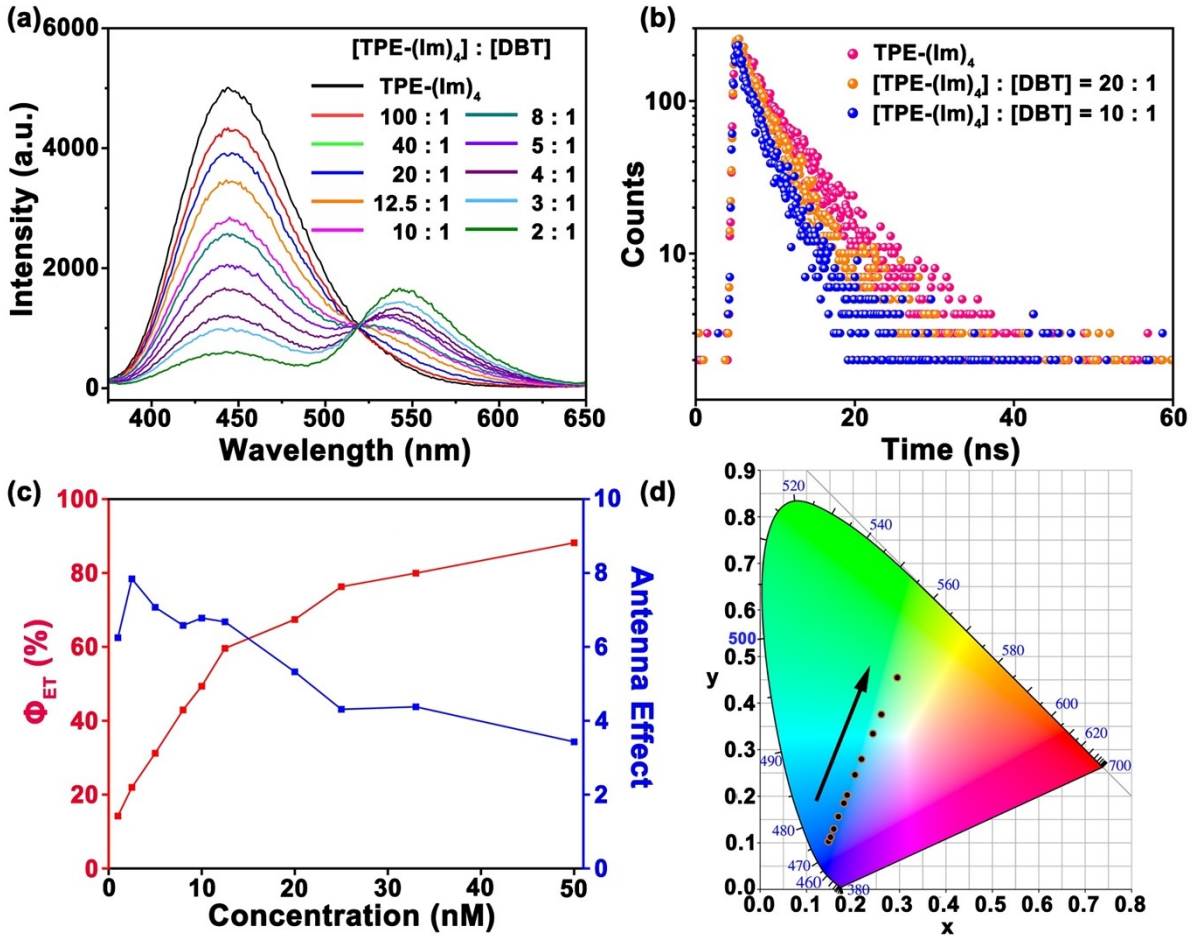

Fig. S56. (a) Fluorescence emission spectra of TPE-$(Im)_4$ & DBT ⊂ PH1 in THF/H_2O mixed solvent. (Experimental conditions: λ_{ex} = 330 nm; slit widths: ex 5 nm, em 2.5 nm; [pillar[5]arene unit] = 10 μM; [TPE-$(Im)_4$] = 1 μM; [DBT] = 0, 10, 25, 50, 80, 100, 125, 200, 250, 333, 500

nM; 25 °C; f_w = 90%). (b) Fluorescence decay profiles of and TPE-$(Im)_4$ ⊂ PH1 (pink dot) and TPE-$(Im)_4$ & DBT ⊂ PH1 amphiphilic polymer carrier with D/A ratio of 20 (orange dot) and 10 (blue dot) monitored at 445 nm. (c) Φ_{ET} and AE of TPE-$(Im)_4$ & DBT ⊂ PH1 with different DBT concentrations. (d) Fluorescence emission spectra of TPE-$(Im)_4$ & DBT ⊂ PH1 supramolecular micelles with different D/A ratios depicted in CIE coordinates.

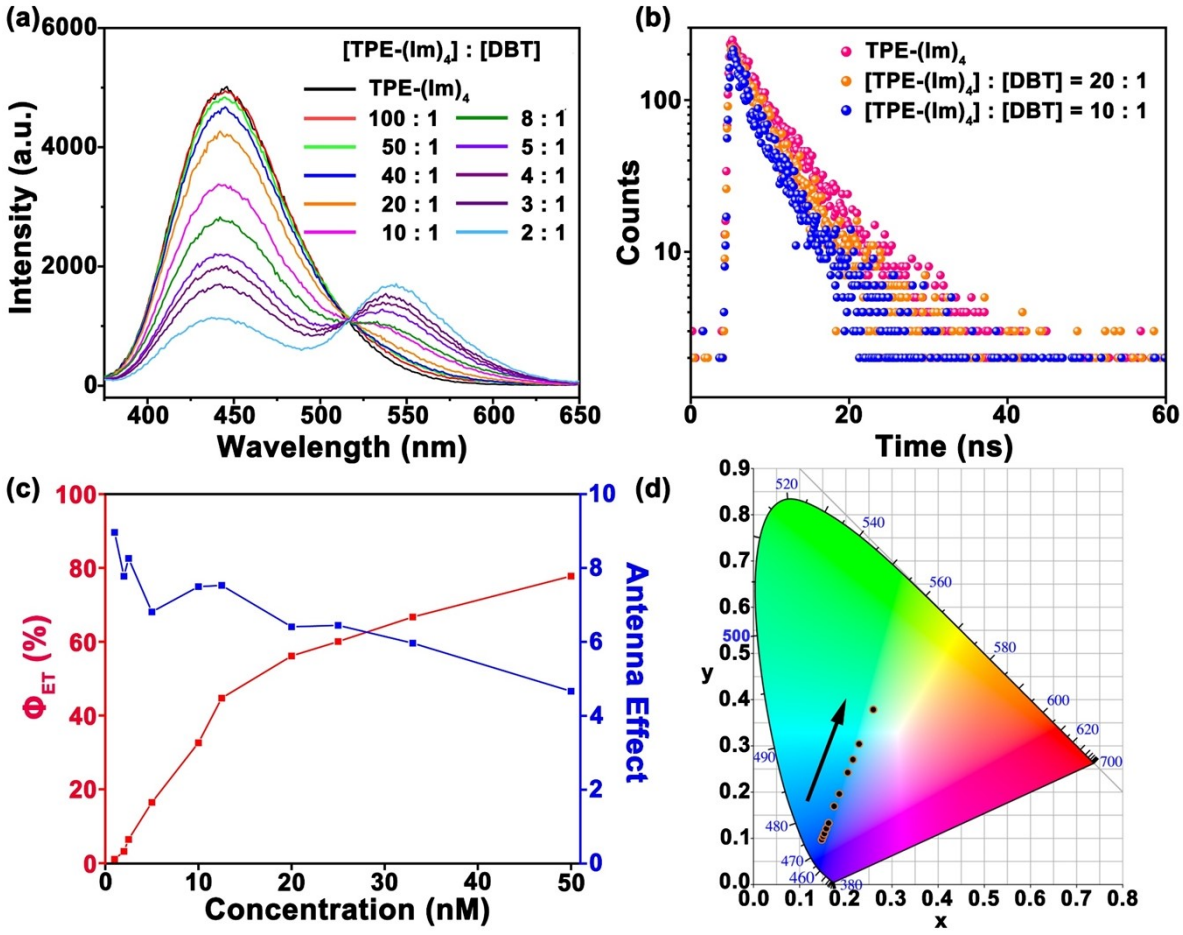

Fig. S57. (a) Fluorescence emission spectra of TPE-$(Im)_4$ & DBT ⊂ PH3 in THF/H_2O mixed solvent. (Experimental conditions: λ_{ex} = 330 nm; slit widths: ex 5 nm, em 2.5 nm; [pillar[5]arene unit] = 10 μM; [TPE-$(Im)_4$] = 1 μM; [DBT] = 0, 10, 20, 25, 50, 100, 125, 200, 250, 333, 500 nM; 25 °C; f_w = 90%). (b) Fluorescence decay profiles of and TPE-$(Im)_4$ (pink dot) and TPE-$(Im)_4$ & DBT⊂PH1 amphiphilic polymer carrier with D/A ratio of 20 (orange dot) and 10 (blue dot) monitored at 445 nm. (c) Φ_{ET} and AE of TPE-$(Im)_4$ & DBT ⊂ PH3 with different DBT

concentrations. (d) Fluorescence emission spectra of TPE-$(Im)_4$ & DBT ⊂ PH3 supramolecular vesicles with different D/A ratios depicted in CIE coordinates.

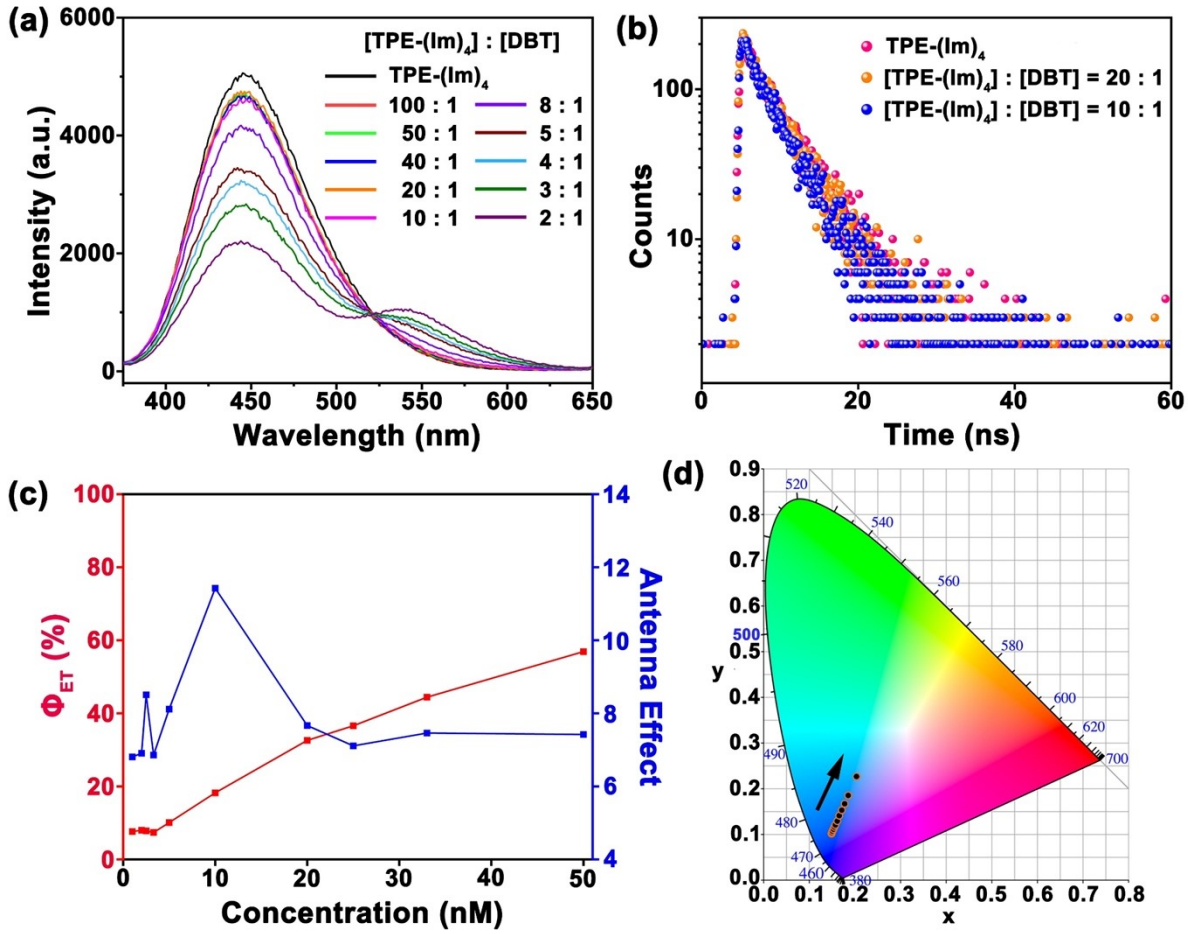

Fig. S58. (a) Fluorescence emission spectra of TPE-$(Im)_4$ & DBT ⊂ PH1 in THF/H_2O mixed solvent. (Experimental conditions: λ_{ex} = 330 nm; slit widths: ex 5 nm, em 2.5 nm; [pillar[5]arene unit] = 10 μM; [TPE-$(Im)_4$] = 1 μM; [DBT] = 0, 10, 20, 25, 50, 100, 125, 200, 250, 333, 500 nM; 25 °C; f_w = 80%). (b) Fluorescence decay profiles of and TPE-$(Im)_4$ ⊂ PH1 (pink dots) and TPE-$(Im)_4$ & DBT ⊂ PH1 amphiphilic polymer carrier with D/A ratio of 20 (orange dots) and 10 (blue dots) monitored at 445 nm. (c) Φ_{ET} and AE of TPE-$(Im)_4$ & DBT ⊂ PH1 with different DBT concentrations. (d) Fluorescence emission spectra of TPE-$(Im)_4$ & DBT ⊂ PH1 supramolecular assembly with different D/A ratios depicted in CIE coordinates.

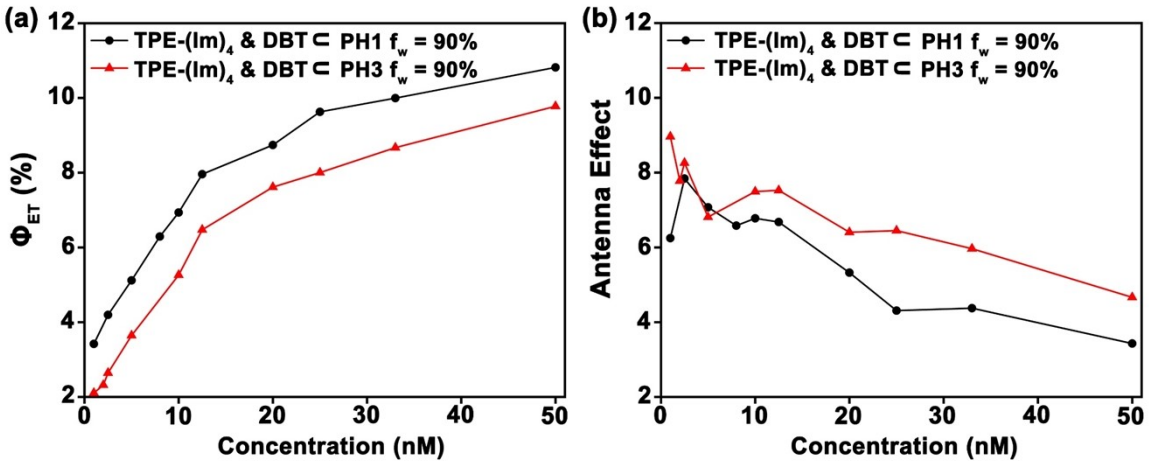

Fig. S59. (a) Φ_{ET} of TPE-$(Im)_4$ & DBT ⊂ PH1 (black line) and TPE-$(Im)_4$ & DBT ⊂ PH3 (red line) in THF/H_2O mixed solvent with f_w of 90%. (b) AE values of TPE-$(Im)_4$ & DBT ⊂ PH1 (black line) and TPE-$(Im)_4$ & DBT ⊂ PH3 (red line) in THF/H_2O mixed solvent with f_w of 90%.

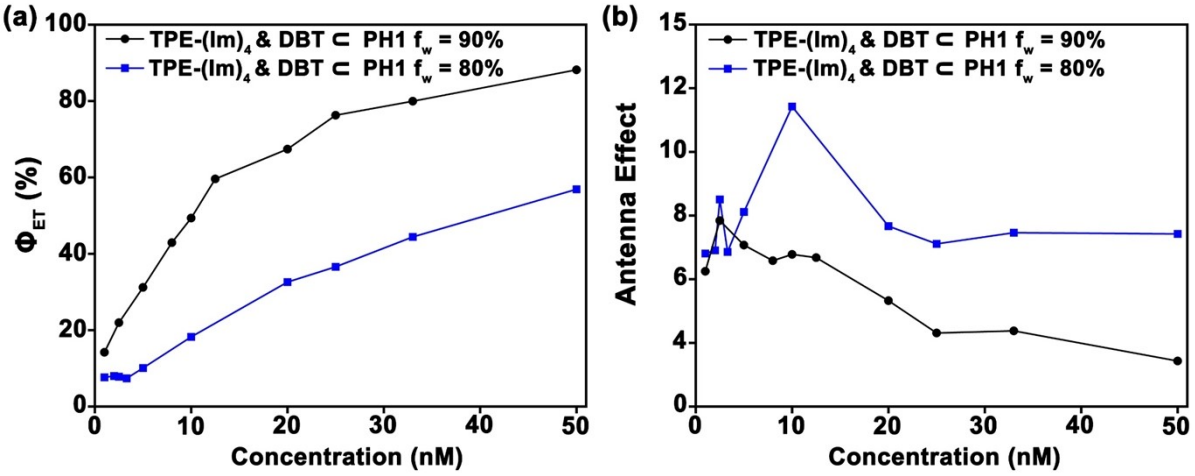

Fig. S60. (a) Φ_{ET} of TPE-$(Im)_4$ & DBT ⊂ PH1 in THF/H_2O mixed solvent with f_w of 90% (black line) and 80 % (blue line). (b) AE values of TPE-$(Im)_4$ & DBT ⊂ PH1 in THF/H_2O mixed solvent with f_w of 90% (black line) and 80 % (blue line).

Table S1. Φ_{ET} and AE values of TPE-$(Im)_4$ & DBT ⊂ PH4 with f_w of 90%

[pillar[5]arene unit]	[TPE-$(Im)_4$]	[DBT]	Φ_{ET}	AE
10 μM	1 μM	0	—	—
10 μM	1 μM	5 nM	4.5	2.3
10 μM	1 μM	10 nM	13.5	4.4
10 μM	1 μM	20 nM	20.5	6.7
10 μM	1 μM	25 nM	24.3	7.5
10 μM	1 μM	50 nM	38.7	6.9
10 μM	1 μM	80 nM	43.9	6.4
10 μM	1 μM	100 nM	51.7	5.6
10 μM	1 μM	125 nM	59.9	5.7
10 μM	1 μM	200 nM	71.6	5.5
10 μM	1 μM	250 nM	76.1	4.3
10 μM	1 μM	333 nM	81.3	3.8
10 μM	1 μM	500 nM	89	3.1

Table S2. Φ_{ET} and AE values of TPE-$(Im)_4$ & DBT ⊂ PH1 with f_w of 90%

[pillar[5]arene unit]	[TPE-$(Im)_4$]	[DBT]	Φ_{ET}	AE
10 μM	1 μM	0	—	—
10 μM	1 μM	10 nM	14.2	6.3
10 μM	1 μM	25 nM	22.0	7.8
10 μM	1 μM	50 nM	31.2	7.1
10 μM	1 μM	80 nM	42.9	6.6
10 μM	1 μM	100 nM	49.3	6.8
10 μM	1 μM	125 nM	59.6	6.7
10 μM	1 μM	200 nM	67.4	5.3
10 μM	1 μM	250 nM	76.3	4.3
10 μM	1 μM	333 nM	80.0	4.4
10 μM	1 μM	500 nM	88.2	3.4

Table S3. Φ_{ET} and AE values of TPE-$(Im)_4$ & DBT ⊂ PH3 with f_w of 90%

[pillar[5]arene unit]	[TPE-$(Im)_4$]	[DBT]	Φ_{ET}	AE
10 μM	1 μM	0	—	—
10 μM	1 μM	10 nM	1.1	9.0
10 μM	1 μM	20 nM	3.2	7.8
10 μM	1 μM	25 nM	6.4	8.3
10 μM	1 μM	50 nM	16.4	6.8
10 μM	1 μM	100 nM	32.6	7.5
10 μM	1 μM	125 nM	44.7	7.5
10 μM	1 μM	200 nM	56.1	6.4
10 μM	1 μM	250 nM	60.0	6.4
10 μM	1 μM	333 nM	66.7	6.0
10 μM	1 μM	500 nM	77.8	4.7

Table S4. Φ_{ET} and AE values of TPE-$(Im)_4$ & DBT ⊂ PH1 with f_w of 80%

[pillar[5]arene unit]	[TPE-$(Im)_4$]	[DBT]	Φ_{ET}	AE
10 μM	1 μM	0	—	—
10 μM	1 μM	10 nM	7.6	6.8
10 μM	1 μM	20 nM	8.0	6.9
10 μM	1 μM	25 nM	7.8	8.5
10 μM	1 μM	33 nM	7.4	6.9
10 μM	1 μM	50 nM	10.1	8.1
10 μM	1 μM	100 nM	18.2	11.4
10 μM	1 μM	200 nM	32.6	7.7
10 μM	1 μM	250 nM	36.6	7.1
10 μM	1 μM	333 nM	44.4	7.5
10 μM	1 μM	500 nM	56.9	7.4

Table S5. Comparison of antenna effects (AE) in different systems.[1-7]

AE	Donor-recipient combination	Provenance
7.5	TPE-$(Im)_4$ & DBT ⊂ PH4	This article
3.6	TPE-$(TA\text{-}CN)_4$ & DSA-$(TA\text{-}CN)_2$ ⊂ poly(MMA-co-MAAm-co-MMAP[5]A)-1	*Adv. Mater.* 2019, *31, 1903962*
12.2	TPE-$(CN)_4$ & DSA-$(TACN)_2$ ⊂ P2 @ F127	*Chem. Eur. J.* 2024, *30*, e202402808
10.1	M-4 (M-DSA-2P[5]A)	*J. Mater. Chem. C*, 2023, *11*, 6607
1.3	RB @ Ga-tpe	*Chem. Sci.* 2023, *14*, 9943
3.7	BDA / TPEM	*J. Am. Chem. Soc.* 2022, *144*, 5389
6.1	TPE-BSBO @ PEI + DBT	*Chem. Commun.* 2023, *59*, 13301
7.8	TPE-SAA + DBT	*Adv. Optical Mater.* 2023, *11*, 2201710
12.3	SOF + DBT + SR101	*J. Mater. Chem. A,* 2023,*11*, 2627

8. Information encryption matrix

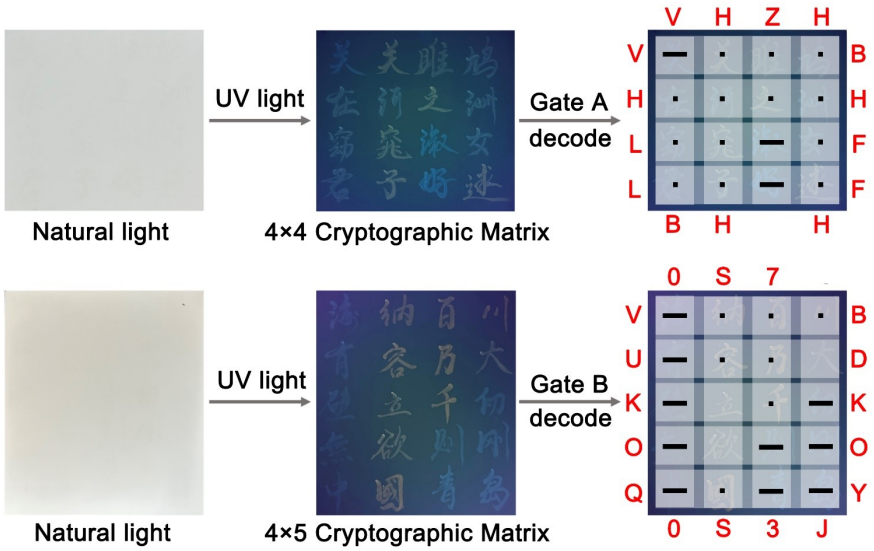

Fig. S61. Schematic illustration of information encryption matrix deciphered by different logic gates which were capable of storing Chinese, English and digits.

References

1. X.-H. Wang, N. Song, W. Hou, C.-Y. Wang, Y. Wang, J. Tang and Y.-W. Yang, *Adv. Mater.* 2019, ***31***, 1903962.
2. Y.-Q. Zhu, Z. Chen, Z.-Y. Chen, Z.-W. Zhou, Q. Bai, M.-X. Wu, X.-H. Wang, *Chem. Eur. J.* 2024, ***30***, e202402808.
3. P.-P. Jia, L. Hu, W.-T. Dou, X.-D. Xu, H. Sun, Z.-Y. Peng, D.-Y. Zhang, H.-B. Yang and L. Xu, *J. Mater. Chem. C*, 2023, ***11***, 6607-6615.
4. D. Li, L. Yang, W. Fang, X. Fu, H. Li, J. Li, X. Li and C. He, *Chem. Sci.* 2023, ***14***, 9943-9950.
5. Y.-X. Yuan, J.-H. Jia, Y.-P. Song, F.-Y. Ye, Y.-S. Zheng, and S.-Q. Zang, *J. Am. Chem. Soc.* 2022, ***144***, 5389-5399.
6. X.-L. Li, R.-Z. Zhang, K.-K. Niu., R.-Z. Dong, H. Liu, S.-S. Yu, Y.-B. W. and L.-B. Xing, *Chem. Commun.* 2023, ***59***, 13301-13304.
7. L.-B. Xing, Y. Wang, X.-L. Li, N. Han, C.-Q. Ma, H. Liu, S. Yu, R. Wang, and S. Zhuo, *Adv. Optical Mater.* 2023, ***11***, 2201710.
8. Y. Wang, C.-Q. Ma, X.-L. Li, R.-Z. Dong, H. Liu, R.-Z. Wang, S. Yu and L.-B. Xing, *J. Mater. Chem. A,* 2023, ***11***, 2627-2633.